Abyssal Atlantic circulation during the Last Glacial Maximum: Constraining the ratio between transport and vertical mixing

D. C. Lund,[1] J. F. Adkins,[2] and R. Ferrari[3]

Received 19 March 2010; revised 23 November 2010; accepted 21 December 2010; published 19 March 2011.

[1] The ocean's role in regulating atmospheric carbon dioxide on glacial-interglacial timescales remains an unresolved issue in paleoclimatology. Reduced mixing between deep water masses may have aided oceanic storage of atmospheric CO_2 during the Last Glacial Maximum (LGM), but data supporting this idea have remained elusive. The $\delta^{13}C$ of benthic foraminifera indicate the Atlantic Ocean was more chemically stratified during the LGM, but the nonconservative nature of $\delta^{13}C$ complicates interpretation of the LGM signal. Here we use benthic foraminiferal $\delta^{18}O$ as a conservative tracer to constrain the ratio of meridional transport to vertical diffusivity in the deep Atlantic. Our calculations suggest that the ratio was at least twice as large at the LGM. We speculate that the primary cause was reduced mixing between northern and southern component waters, associated with movement of this water mass boundary away from the zone of intense mixing near the seafloor. The shallower water mass boundary yields an order of magnitude increase in the volume of southern component water, suggesting its residence time may have increased substantially. Our analysis supports the idea that an expanded volume of Antarctic Bottom Water and limited vertical mixing enhanced the abyssal ocean's ability to trap carbon during glacial times.

Citation: Lund, D. C., J. F. Adkins, and R. Ferrari (2011), Abyssal Atlantic circulation during the Last Glacial Maximum: Constraining the ratio between transport and vertical mixing, *Paleoceanography*, *26*, PA1213, doi:10.1029/2010PA001938.

1. Introduction

[2] At the Last Glacial Maximum (LGM; ~20,000 years ago), atmospheric carbon dioxide levels were 80–90 ppm lower than preindustrial values [*Neftel et al.*, 1982; *Monnin et al.*, 2001]. Because more than 90% of the combined oceanic, atmospheric and terrestrial carbon resides in the deep ocean, this reservoir is believed to play a primary role in regulating atmospheric CO_2 on glacial-interglacial timescales [*Broecker*, 1982; *Sigman and Boyle*, 2000]. Since publication of the "Harvardton Bears" box models, it was realized that nutrient utilization and overturning rate in Southern Ocean deep water are two of the key controls on atmospheric CO_2 levels [*Knox and McElroy*, 1984; *Sarmiento and Toggweiler*, 1984; *Siegenthaler and Wenk*, 1984]. *Toggweiler* [1999] refined this view when he speculated that reduced mixing between deep water masses formed in the Southern Ocean and the North Atlantic also helped sequester atmospheric CO_2 during glacial times. Vertical mixing, overturning rate, nutrient status, and volume of the glacial southern source deep water are all thought to be important controls in regulating pCO_2.

[3] Deep ocean nutrient tracers $\delta^{13}C$ and Cd/Ca provide a relatively clear picture of the water mass distribution in the LGM Atlantic. Benthic $\delta^{13}C$ shows that the deep ocean was more isotopically stratified during the LGM (Figure 1) [*Boyle and Keigwin*, 1982; *Curry and Lohmann*, 1982; *Duplessy et al.*, 1988; *Kallel et al.*, 1988; *Herguera et al.*, 1992; *Keigwin*, 2004; *Curry and Oppo*, 2005; *Oppo and Lehman*, 1993]. The distribution of $\delta^{13}C$ in the Atlantic has been explained by invoking changes in transport of Antarctic Bottom Water (AABW) relative to North Atlantic Deep Water (NADW) [*Duplessy et al.*, 1988; *Curry and Oppo*, 2005]. However, tracers like $\delta^{13}C$ also respond to variations in water mass mixing, variations in surface air-sea fluxes, and nonconservative behavior. In this paper, we use $\delta^{18}O$ and $\delta^{13}C$ data in an attempt to better quantify the relative roles of transport, vertical mixing, and remineralization in the abyssal Atlantic.

[4] Efforts to reconstruct the deep circulation using $\delta^{13}C$ may be hindered by the fact that $\delta^{13}C$ is a nonconservative tracer; its distribution is affected not only by the ocean circulation but also the biological remineralization of organic matter. Organic carbon created by phytoplankton in the surface ocean is depleted in its $^{13}C/^{12}C$ ratio relative to dissolved inorganic carbon (DIC). As organic matter falls through the water column, remineralization at depth produces ^{13}C-depleted DIC that is incorporated in the shells of benthic foraminifera. This process masks the effect of circulation and mixing on the $\delta^{13}C$ tracer field. A conservative tracer, that is, one which is influenced only by transport and mixing, is needed if one is to attempt a reconstruction of the deep ocean circulation from tracer profiles.

[1]Department of Geological Sciences, University of Michigan, Ann Arbor, Michigan, USA.
[2]Division of Geological and Planetary Sciences, California Institute of Technology, Pasadena, California, USA.
[3]Department of Earth, Atmospheric, and Planetary Sciences, Massachusetts Institute of Technology, Cambridge, Massachusetts, USA.

0883-8305/11/2010PA001938

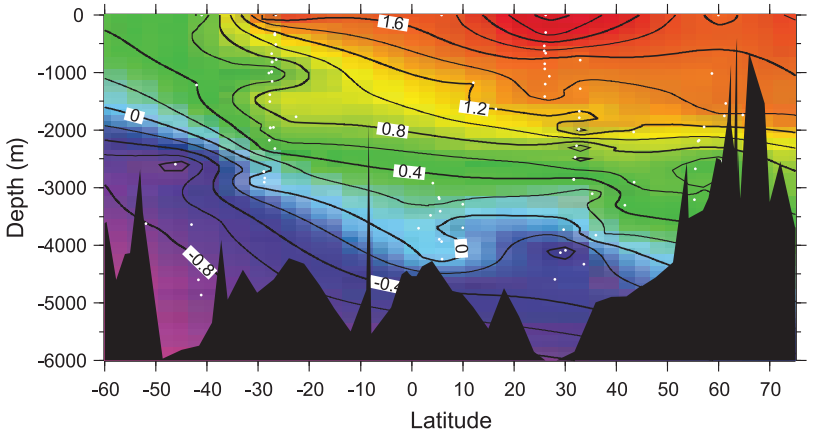

Figure 1. Contour map of benthic foraminiferal $\delta^{13}C$ for the Western Atlantic during the Last Glacial Maximum [*Curry and Oppo*, 2005]. The strong vertical gradient in $\delta^{13}C$ could be due to (1) enhanced remineralization of organic carbon at depth, (2) greater transport of AABW relative to northern component water, (3) reduced mixing between AABW and northern component water, or (4) some combination of these effects.

[5] The stable oxygen isotopic ratio of foraminifera ($\delta^{18}O_c$) varies as a function temperature and the $\delta^{18}O$ of seawater, which is directly related to salinity. Because both temperature and salinity are conservative tracers, so too is $\delta^{18}O_c$. In the upper ocean, $\delta^{18}O_c$ can be used as a proxy for seawater density because both parameters have a linear dependence on temperature and salinity [*Lynch-Stieglitz et al.*, 1999]. In the deep ocean, however, this relationship breaks down because seawater density varies nonlinearly with temperature. Furthermore, the $\delta^{18}O$-seawater relationship can vary between water masses and on glacial-interglacial timescales [*Zahn and Mix*, 1991]. Instead of estimating paleo-densities for the abyss, here we simply exploit the conservative nature of $\delta^{18}O_c$. Once $\delta^{18}O_c$ is set at the surface, the value is conserved by a water parcel as it moves into the ocean interior; $\delta^{18}O_c$ can only be modified by mixing and transport. A minor caveat is that in situ temperature recorded by foraminifera is not truly conservative because it can be changed through compressive effects. However, this effect is negligible for the present study as we show below.

1.1. The $\delta^{18}O$ Evidence for an Abyssal Water Mass Boundary

[6] The strong vertical gradient in North Atlantic Ocean benthic foraminiferal $\delta^{13}C$ is a well-known feature of the LGM ocean. Less well recognized is that LGM benthic $\delta^{18}O$ (we use $\delta^{18}O$ as shorthand for $\delta^{18}O_c$ for the remainder of the paper) profiles also have a larger gradient with water depth than today (Figure 2). At the Brazil Margin (30°S), the change in *Cibicidoides* $\delta^{18}O$ between 1 and 3 km was approximately 0.3‰ larger during the LGM (Figure 2a) [*Curry and Oppo*, 2005]. The $\delta^{18}O$ gradient is most easily observed in the difference between LGM and Holocene profiles (Figure 2b). The larger LGM gradient also exists in $\delta^{18}O$ data from the Blake Ridge (30°N), where it is observed in two genera of benthic foraminifera, *Cibicidoides* and *Uvigerina* (Figure 2d). At each location, the LGM-Holocene $\delta^{18}O$ pattern is driven by a larger increase in LGM $\delta^{18}O$ below ~2 km. Similar patterns have been observed in the Indian [*Kallel et al.*, 1988] and Pacific Oceans [*Herguera et al.*, 1992] suggesting the LGM "step" in $\delta^{18}O$ may have been a global feature.

1.2. Diagnosing the Transport to Mixing Ratio From Tracer Distributions

[7] A detailed analysis of the processes that influence $\delta^{18}O$ is necessary to identify what generates the observed differences in the LGM and modern data. The distributions of tracers in the ocean are set through a balance between advection (e.g., by the overturning circulation), air-sea fluxes at the surface, and mixing in the ocean interior. The overturning circulation of AABW in the Atlantic Ocean is associated with sinking of water through convection around Antarctica and a return flow at shallower levels. The properties of AABW are set by surface fluxes near Antarctica and mixing with overlying waters in the ocean interior. Air-sea fluxes have been used to estimate water mass transport in the present climate [*Schlosser et al.*, 1991; *Speer and Tziperman*, 1992; *Large and Nurser*, 2001], but this type of data is lacking in the paleoclimate record. Instead, we infer the ratio between meridional transport and vertical diffusivity in the abyss from tracer distributions. AABW is uniquely suited to this approach because it does not outcrop north of Drake Passage and it is only modified through mixing with other water masses.

[8] Reconstructing the ocean circulation from tracer distributions is often necessary when tracer data are more readily available than velocity measurements. Using the inverse approach, *Wunsch* [1996] shows how to combine tracer measurements to constrain ocean circulation with least square techniques: the larger the set of measurements, the smaller the uncertainty on the inferred circulations and fluxes. Inversions with available LGM data from the Atlantic have been used to evaluate whether the modern circulation is the same as the past [*LeGrand and Wunsch*,

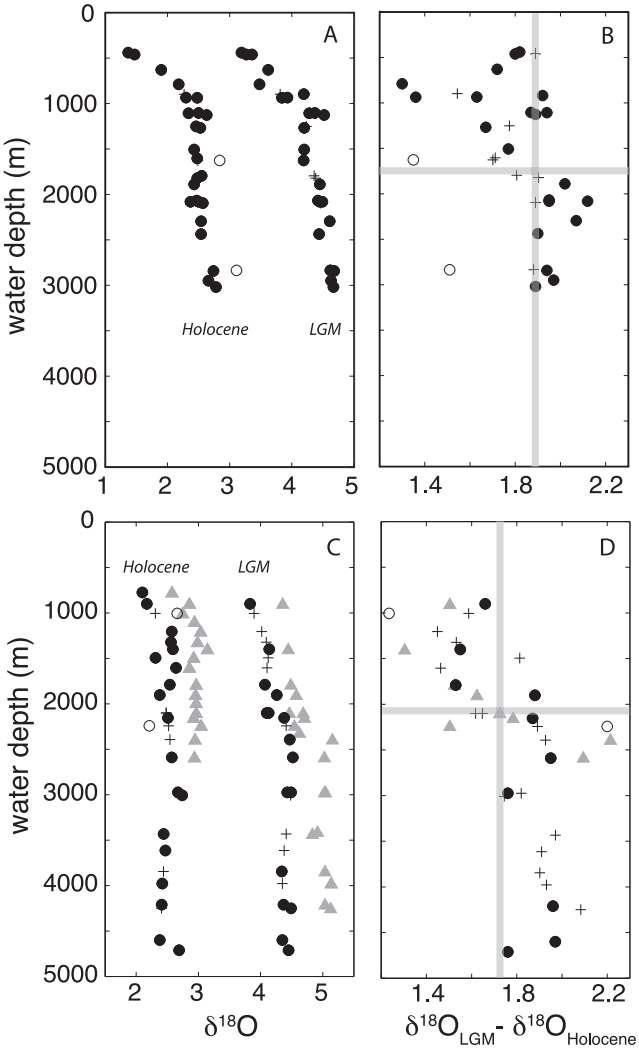

Figure 2. (a) Brazil Margin *Cibicidoides spp.* δ^{18}O (solid circles) [*Curry and Oppo*, 2005], outliers (open circles), and interpolated data points (crosses). Outliers are defined as those values which exceed the mean δ^{18}O from adjacent water depths by more than ±0.3‰. Interpolated values are based on linear interpolation between data points at adjacent water depths. (b) Brazil Margin LGM-Holocene δ^{18}O. (c) Blake Ridge *Cibicidoides spp.* δ^{18}O (solid circles) [*Keigwin*, 2004], outliers (open circles), and interpolated data points (crosses). Also included are *Uvigerina spp.* δ^{18}O (gray triangles) [*Keigwin*, 2004]. (d) Blake Ridge LGM-Holocene δ^{18}O. Using a Student *t* test and assuming a threshold two-sided *p* value of 0.05, we are able to reject the null hypothesis that the shallow and deep LGM-Holocene δ^{18}O data are sampled from the same population ($p \cong 0.005$ for Brazil Margin *Cibicidoides sp.*, $p \cong 0.0005$ for Blake Ridge *Cibicidoides sp.*, and $p \cong 0.02$ for Blake Ridge *Uvigerina sp.*). This result is not surprising given that LGM-Holocene δ^{18}O data above 2 km fall in the upper left-hand quadrant of each plot, while the deeper data fall in the lower right-hand quadrant.

1995; *Gebbie and Huybers*, 2006; *Marchal and Curry*, 2008]. Here we acknowledge that the data are too sparse to uniquely constrain the LGM circulation field and we set a more modest goal. We instead evaluate which transport to vertical mixing ratio for AABW is consistent with the available δ^{18}O data. We assume that the few available profiles are representative of an entire basin and evaluate the implications. This exercise is informative because it highlights the key factors that influence δ^{18}O and δ^{13}C profiles in the modern and LGM Atlantic. The question of whether our results apply to the entire Atlantic Ocean will have to wait until more stable isotopic profiles are available. A recent inverse calculation for the LGM Atlantic by *Marchal and Curry* [2008] focused on estimating the consistency of LGM data with the modern circulation. Our analysis differs from this work in two important ways. First, we only attempt to constrain the ratio of Ψ/κ for the glacial southern source water mass, not the circulation of the entire basin. Second, we explicitly consider vertical mixing in our analysis whereas the previous work treated this term implicitly as an error in the tracer budget. Overall our goal is less ambitious than a full tracer inversion, but our data set is also more limited. We see these two approaches as complimentary in the goal to better understand the role of the deep ocean in glacial-interglacial climate change.

2. Methods

2.1. Tracer Budget for δ^{18}O

[9] In this section, we provide an abbreviated description of the tracer budget for δ^{18}O and δ^{13}C. The full derivation is given in Appendix A. Our tracer budget encompasses the volume of water below a surface of constant tracer concentration, as shown in Figure 3, departing from the traditional approach that considers volumes below a fixed depth. The advantage is that the net amount of tracer flowing into such a volume from the south can only be balanced by mixing of tracer across the upper surface. By construction, the mean circulation advects tracer into the volume from the south, but it cannot flux tracer across a contour. Consider the conservative tracer δ^{18}O. At the order of magnitude level, the transport of δ^{18}O from the south is given by the maximum of the zonally averaged overturning circulation, Ψ ($m^3\ s^{-1}$), multiplied by the difference in tracer at the top and bottom of our control volume, $\Delta\delta^{18}$O (‰). The transport of tracer into the South Atlantic is balanced by mixing with overlying waters giving

$$2/3\Psi\Delta\delta^{18}\mathrm{O} \approx \kappa\delta^{18}\mathrm{O}_z A \qquad (1)$$

where the right hand side represents the diffusion of tracer expressed as a turbulent diffusivity, κ ($m^2\ s^{-1}$), times the vertical tracer gradient at the upper boundary of AABW, $\delta^{18}O_z$ (‰ m^{-1}), and A is the area across which mixing occurs (m^2). The scaling factor of 2/3 accounts for the fact that the top of our control volume corresponds to the maximum overturning stream function and therefore our budget

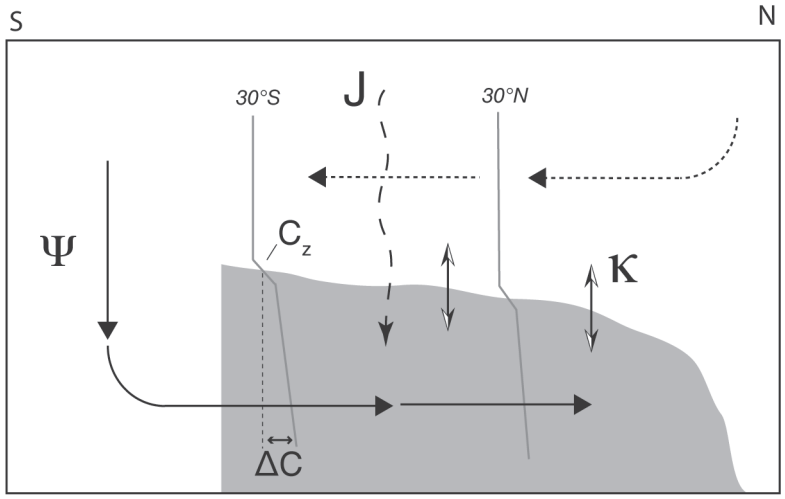

Figure 3. Two-dimensional representation of the transport and mixing of a generic tracer (C) in the abyssal Atlantic. In reality, the tracer surface varies in three dimensions. The tracer budget is computed for volumes north of 27°S and below a constant tracer value. C_z is the vertical tracer gradient at the upper lid of AABW, and ΔC is the difference in C between the tracer surface and the seafloor. A conservative tracer like $\delta^{18}O$ is affected by transport (Ψ) from the Southern Ocean (solid arrow) and vertical mixing (κ) with overlying waters. The horizontal dashed arrow represents transport of northern component water. A nonconservative tracer like $\delta^{13}C$ is also affected by J, the remineralization of organic matter (dashed vertical arrow). Our approach depends on tracer distributions in the ocean interior (gray areas) distant from the water mass outcropping region near Antarctica.

does not include southward advection out of the Atlantic (see Appendix A). It is useful to rearrange the budget so that quantities that can be estimated from observations are on the right hand side and unknowns are on the left:

$$\frac{\Psi}{\kappa} \approx \frac{3}{2}\frac{\delta^{18}O_z}{\Delta\delta^{18}O}A \tag{2}$$

In other words, we can describe the ratio of tracer transport (Ψ) to vertical mixing of tracer (κ) using vertical gradients in the $\delta^{18}O$ profiles, the vertical difference $\Delta\delta^{18}O$, and the area of the $\delta^{18}O$ isosurface. By comparing the modern and LGM estimates of this ratio, we can evaluate the relative importance of transport to vertical mixing through time.

[10] Our tracer budget approach is similar to W. Munk's local balance between upwelling and mixing in his classic paper "Abyssal Recipes" [*Munk*, 1966]. We differ from this approach by balancing the total transport of tracer within a water mass against mixing with other waters. In essence, we swap local upwelling (w, m/s) and mixing (κ, m^2/s) for the integrated volume transport (Ψ, m^3/s) and the mixing integrated over the whole upper 'lid' of the water mass ($A\kappa$, m^4/s). This difference is crucial, because a local vertical balance rarely holds in the ocean.

2.2. Tracer Budget for $\delta^{13}C$

[11] The budget describing the distribution of $\delta^{13}C$ in the abyssal Atlantic (Figure 3) differs from that of $\delta^{18}O$ in that it has the additional contribution of a biological remineralization term, J (‰ s^{-1}), multiplied by the volume into which the remineralization occurs, V (m^3):

$$2/3\Psi\Delta\delta^{13}C + JV \approx \kappa\delta^{13}C_z A \tag{3}$$

where $\Delta\delta^{13}C$ is the difference in $\delta^{13}C$ between water entering the South Atlantic and $\delta^{13}C$ of the upper 'lid' of AABW, defined as the maximum in the overturning stream function. $\delta^{13}C_z$ is the gradient in $\delta^{13}C$ at the upper boundary of AABW. In this equation, we place the sink terms on the left-hand side of the equation, and the source term on the right. Ψ is positive and acts as a sink of $^{13}C/^{12}C$ for the abyssal cell, because incoming AABW has a low $^{13}C/^{12}C$ ratio. J is also a sink, as organic matter is strongly depleted in ^{13}C. The diffusive term is a source, since mixing with northern component water adds dissolved inorganic carbon with a higher $^{13}C/^{12}C$ ratio than AABW. Dividing through by the diffusive flux and rearranging the terms, we obtain:

$$Pe \equiv \frac{2}{3}\frac{\Psi}{\kappa}\frac{\Delta\delta^{13}C}{\delta^{13}C_z A} = \frac{\delta^{18}O_z}{\Delta\delta^{18}O}\frac{\Delta\delta^{13}C}{\delta^{13}C_z} = 1 - \frac{Jh}{\kappa\delta^{13}C_z} \tag{4}$$

where h is the vertical extent of the volume considered, that is, $V = Ah$. The first term is a bulk Peclet number, *Pe*, the nondimensional ratio of tracer transport to tracer diffusion. We use a bulk *Pe* because we focus on the zonally integrated advection (i.e., transport) of tracer. *Pe* can be estimated using Ψ/κ from the $\delta^{18}O$ tracer budget and $\Delta\delta^{13}C$ and $\delta^{13}C_z$ derived from the $\delta^{13}C$ profiles. With substitution we see that

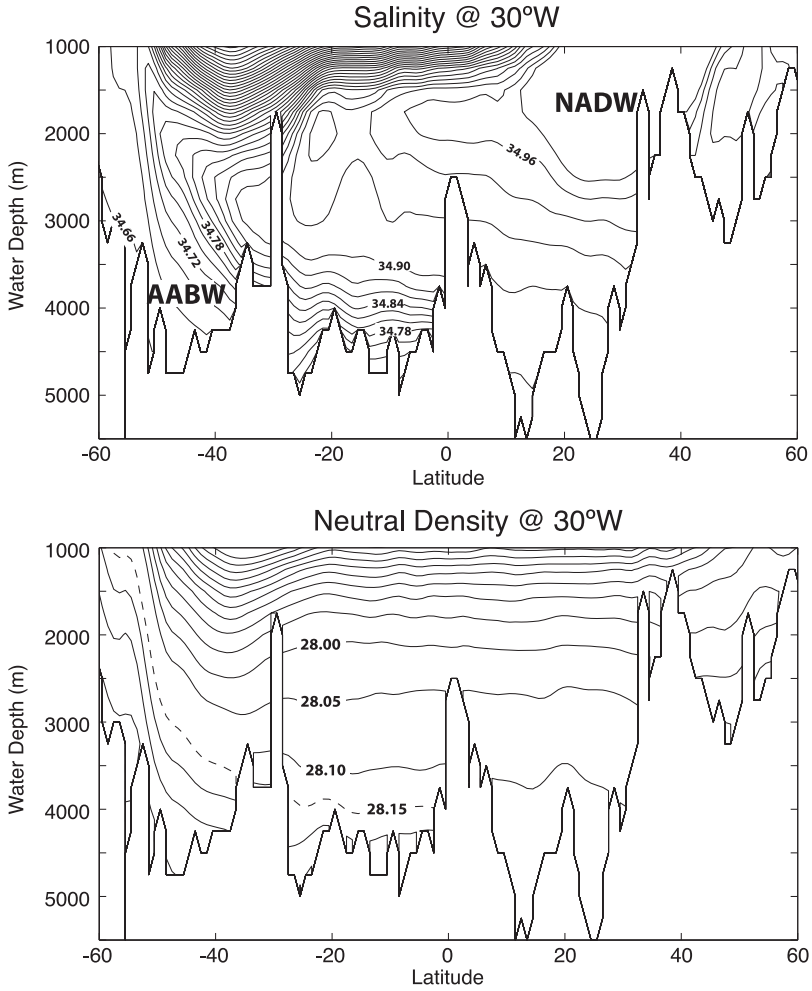

Figure 4. (top) Salinity section along 30°W in the Atlantic Ocean. The contour interval is 0.02 salinity units. The largest vertical gradient in salinity in the deep Atlantic between 30°S and the equator exists from 3800 to 4300 m water depth, the approximate location of the upper boundary for AABW. (bottom) Neutral density section along 30°W in the Atlantic Ocean. The maximum vertical salinity gradient corresponds to a neutral density surface $\gamma = 28.15$ kg/m^3 (dashed line), which also marks the maximum overturning stream function for the South Atlantic [*Lumpkin and Speer*, 2007]. Salinity and neutral density data are from the WOCE Global Hydrographic Climatology [*Gouretski and Koltermann*, 2004].

Pe is only dependent on the tracer distribution and not the volume or the area. The nonconservative term J can only make *Pe* smaller. In section 3, we evaluate modern and LGM δ^{18}O and δ^{13}C profiles that sample southern source water. We also check that our tracer balance for the modern ocean gives a value of Ψ that is consistent with other estimates. In section 4 we evaluate the Ψ/κ and *Pe* values implied by these results and comment on their implications.

3. Results

3.1. Modern δ^{18}O Budget

[12] Does the δ^{18}O tracer budget described above yield reasonable Ψ/κ values for the modern AABW circulation in the Atlantic? To answer this question, we first need to outline the δ^{18}O domain for our analysis. Ideally, the δ^{18}O surface that defines our control volume should coincide with the upper boundary of AABW. Here we define the upper boundary for AABW as the neutral density surface $\gamma = 28.15$ kg/m^3, which ranges from 3000 to 4000 m water depth in the South Atlantic and corresponds to the maximum vertical salinity gradient (Figure 4). The $\gamma = 28.15$ kg/m^3 surface coincides with the maximum overturning stream function in the abyssal South Atlantic; the net flow of water below $\gamma = 28.15$ kg/m^3 is northward, while flow above $\gamma = 28.15$ kg/m^3 is primarily southward [*Lumpkin and Speer*, 2007]. For consistency with the LGM budget, we set the southern edge of our domain at 27°S, the approximate latitude of the Brazil Margin cores [*Curry and Oppo*, 2005].

[13] Today, AABW sits below the deepest core sites at Brazil Margin. As a result, our modern δ^{18}O budget must rely on estimates of the equilibrium δ^{18}O of calcite calculated from temperature and seawater δ^{18}O data. We created a data set of gridded calcite δ^{18}O based on the δ^{18}O of

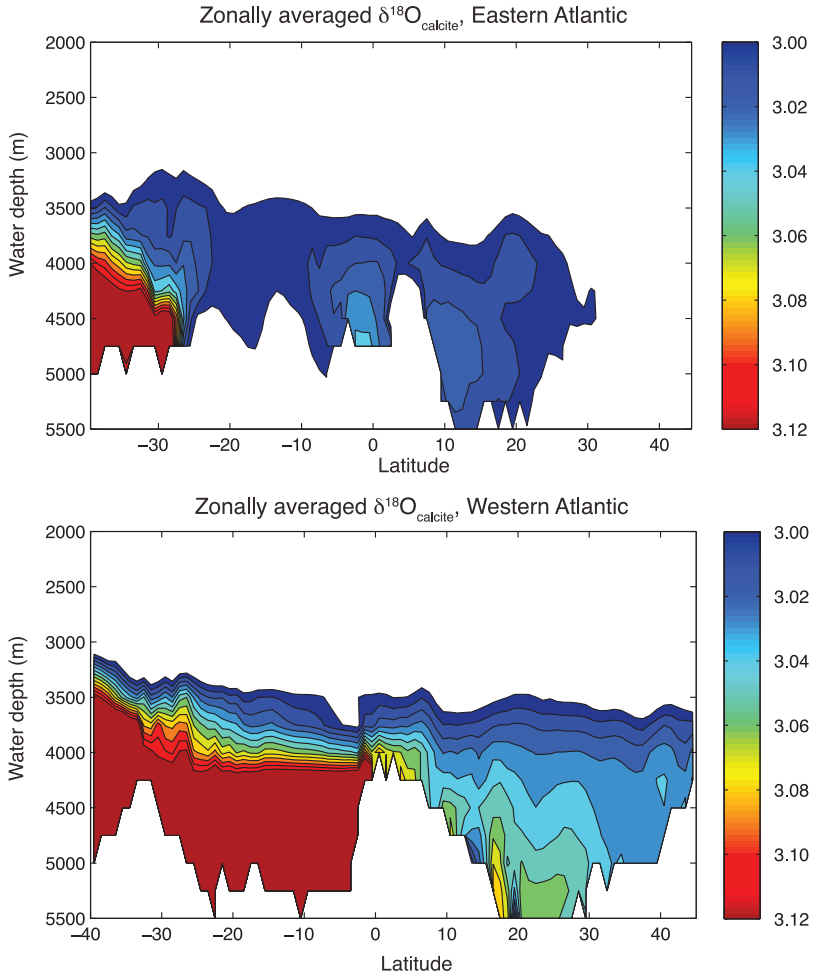

Figure 5. Contoured map of zonally averaged $\delta^{18}O$ for the (top) eastern Atlantic and (bottom) western Atlantic. The gridded data set was created using a $\delta^{18}O$ of seawater database [*LeGrande and Schmidt*, 2006], WOCE Global Hydrographic Climatology temperatures [*Gouretski and Koltermann*, 2004], and a paleotemperature equation [*Kim and O'Neil*, 1997] adjusted for an acid fractionation factor of 1.0105. Delta^{18}O values exceeding 3.08‰ exist primarily in the southwestern Atlantic where the influence of AABW is most pronounced.

seawater database [*LeGrande and Schmidt*, 2006], in situ temperatures from the WOCE Global Hydrographic Climatology [*Gouretski and Koltermann*, 2004] and a paleotemperature equation [*Kim and O'Neil*, 1997] modified for an acid-fractionation factor of 1.0105. Sections of equilibrium $\delta^{18}O$ of calcite for the western and eastern Atlantic are shown in Figure 5. The Atlantic AABW end-member has $\delta^{18}O$ values $\geq$ 3.12‰ while the NADW end-member has $\delta^{18}O$ values $\leq$ 3.00‰. Because $\delta^{18}O$ is conservative, the maximum vertical gradient in $\delta^{18}O$ ($\delta^{18}O_z$) should mark the approximate boundary between AABW and NADW.

[14] We calculated $\delta^{18}O_z$ for all grid points north of 27°S using $\delta^{18}O$ estimates from immediately above and below a given $\delta^{18}O$ horizon, over a span of 500 m water depth. A plot of $\delta^{18}O_z$ across $\delta^{18}O$ surfaces from 3.00‰ to 3.20‰ is shown in Figure 6. The maximum in $\delta^{18}O_z$ occurs for values between 3.06‰ to 3.10‰. These $\delta^{18}O$ surfaces track very closely the $\gamma = 28.15$ kg/m^3 surface and provide an objective method to identify the upper boundary of AABW in the Atlantic from $\delta^{18}O$ profiles. Figure 6 also shows the vertical gradient in potential temperature and salinity across the $\delta^{18}O$ isosurfaces, calculated using the WOCE Global Hydrographic Climatology [*Gouretski and Koltermann*, 2004]. We take vertical differences across 250 m, the resolution of the climatology. The maximum vertical gradients in T and S correspond to the maximum in $\delta^{18}O_z$, confirming that $\delta^{18}O$ acts as a conservative tracer that tracks the upper boundary of AABW. We choose $\delta^{18}O$ = 3.08‰ to define our modern control volume for AABW. This $\delta^{18}O$ surface has an average $\delta^{18}O_z$ of $(-3.1 \pm 0.8) \times 10^{-4}$‰ m^{-1} ($\pm 1\sigma$) (Figure 7). The $\delta^{18}O$ surfaces ranging from 3.06‰ to 3.11‰ have similar $\delta^{18}O_z$ values (Figure 6).

[15] We calculated $\Delta\delta^{18}O$ for the modern by subtracting the $\delta^{18}O$ values nearest the seafloor at 27°S from the $\delta^{18}O$ value = 3.08‰ chosen for the upper boundary of our control volume. A cross section of modern $\delta^{18}O$ at 27°S, the

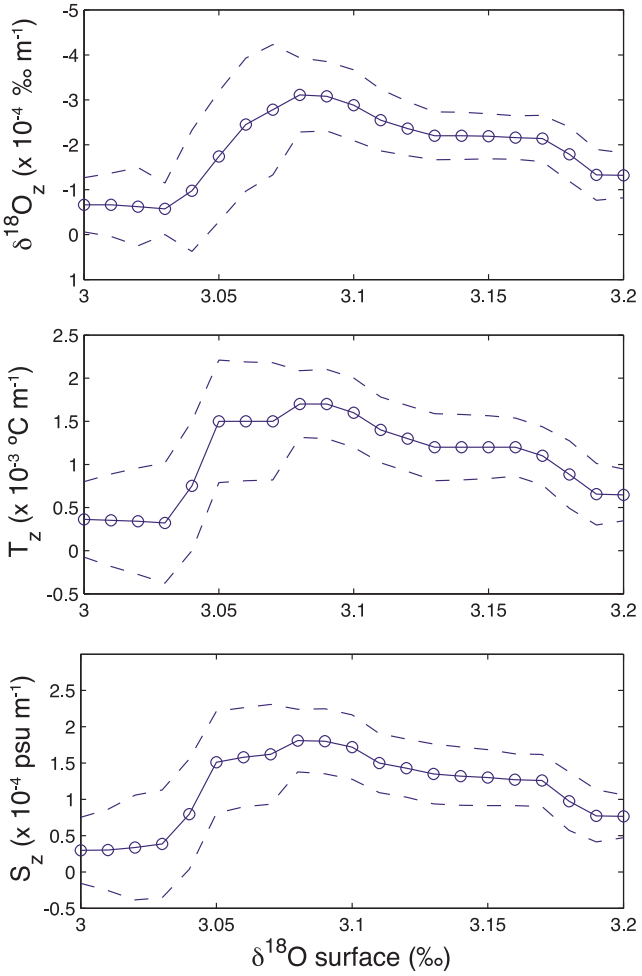

Figure 6. (top) The vertical gradient in $\delta^{18}O$, (middle) potential temperature, and (bottom) salinity across $\delta^{18}O$ isosurfaces ranging from 3.00‰ to 3.20‰. One-sigma standard deviations are given as dashed lines. Temperature and salinity data are from the WOCE Global Hydrographic Climatology [*Gouretski and Koltermann*, 2004]. The maximum $\delta^{18}O_z$ occurs between $\delta^{18}O$ values of 3.06‰ and 3.11‰.

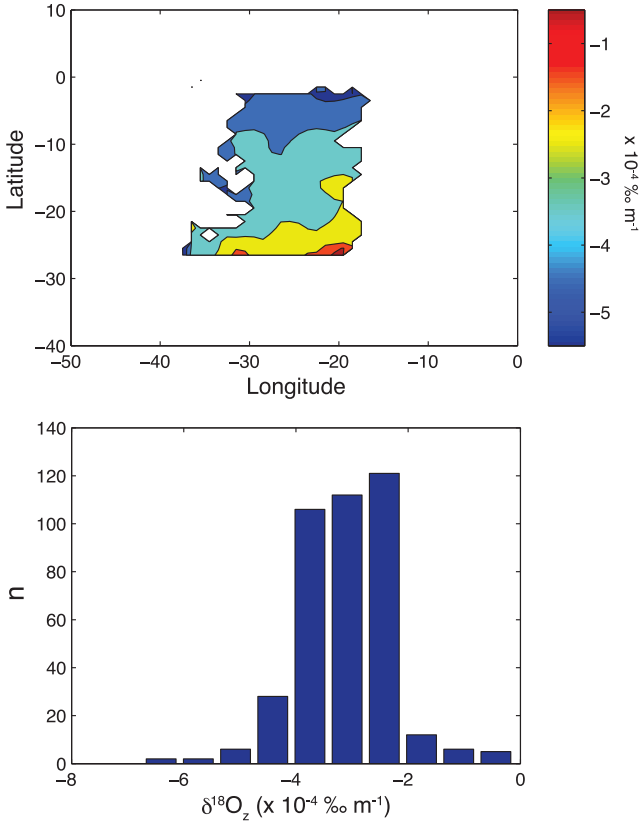

Figure 7. (top) Contour map of the vertical $\delta^{18}O$ gradient ($\delta^{18}O_z$) at $\delta^{18}O$ = 3.08‰. This $\delta^{18}O$ surface spans the southwestern Atlantic. (bottom) Histogram of $\delta^{18}O_z$ values along the $\delta^{18}O$ = 3.08‰ surface in the southwestern Atlantic. The mean $\delta^{18}O_z$ value for this $\delta^{18}O$ surface is -3.1×10^{-4} ‰ m^{-1}.

southern limit of our circulation cell, is shown in Figure 8. At this latitude, there are 21 separate 1° longitude bins across the western Atlantic where the $\delta^{18}O$ value at the seafloor exceeds 3.08‰. We calculated $\Delta\delta^{18}O$ for each bin separately, and then took the average to calculate a $\Delta\delta^{18}O$ of -0.09 ± 0.01‰. If instead we focus on the intense flow along the western boundary where most of the tracer flux occurs, $\Delta\delta^{18}O = -0.15 \pm 0.01$‰. To cover these two different options, we use an intermediate $\Delta\delta^{18}O$ value with an error that encompasses both (-0.12 ± 0.04‰).

[16] Using our estimates of $\delta^{18}O_z$ and $\Delta\delta^{18}O$ and the tracer budget for $\delta^{18}O$ (equation (2)), we estimate $\Psi/\kappa = (1.8 \pm 0.8) \times 10^{10}$ m for the modern $\delta^{18}O$ surface = 3.08‰ (Table 1). We obtain similar Ψ/κ estimates for $\delta^{18}O$ surfaces ranging from 3.06‰ to 3.11‰. Assuming a κ for the deep

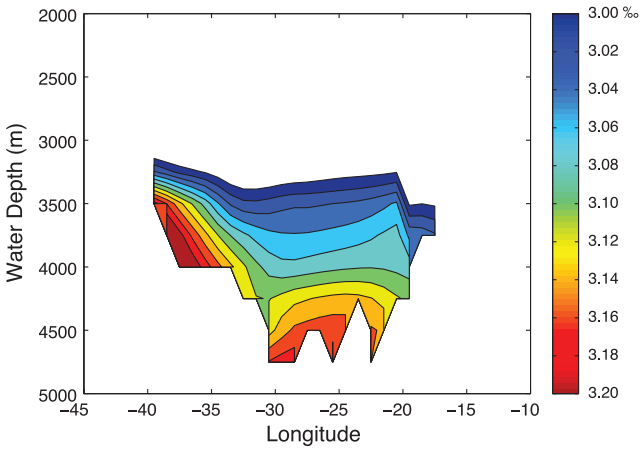

Figure 8. Contoured cross section of $\delta^{18}O$ at 27.5°S in the southwest Atlantic. The $\delta^{18}O$ values are contoured in 0.02‰ increments from 3.00 to 3.20‰. We calculated $\Delta\delta^{18}O$ by subtracting the $\delta^{18}O$ values nearest the seafloor from 3.08‰. $\Delta\delta^{18}O$ is larger if the calculation is limited to the western boundary, where the majority of tracer fluxes into our control volume (see text for details).

Table 1. Parameters for Modern Tracer Budget

Tracer Surface	Vertical Gradient[a] ($\times 10^{-4}$ ‰ m^{-1})	Vertical Difference[b] (‰)	Ratio[c] (m)	Area ($\times 10^{12}$ m^2)	Ψ/κ ($\times 10^{10}$ m)	*Pe*
$\delta^{18}O$ = 3.08‰	−3.1 ± 0.8	−0.12 ± 0.04	390 ± 160	4.7 ± 0.5	1.8 ± 0.8	
$\delta^{13}C$ = 0.70‰	4.8 ± 1.0	0.24 ± 0.05	510 ± 150	4.7 ± 0.5	1.4 ± 0.4	1.3 ± 0.7

[a]Vertical gradients are $\delta^{18}O_z$ and $\delta^{13}C_z$.
[b]Vertical differences are $\Delta\delta^{18}O$ and $\Delta\delta^{13}C$.
[c]Ratios are $\Delta\delta^{18}O/\delta^{18}O_z$ and $\Delta\delta^{13}C/\delta^{13}C_z$.

Atlantic of $(3 \pm 1.5) \times 10^{-4}$ m^2 s^{-1} [*Ganachaud and Wunsch*, 2000], then the tracer-derived AABW transport at 27°S is 5.5 ± 3.7 Sv (1Sv = 1×10^6 m^3 s^{-1}). We obtain a similar Ψ if we use an estimate of κ for the Brazil Basin at the approximate depth of the γ = 28.15 kg/m^3 surface ((3.3 ± 2.4) × 10^{-4} m^2 s^{-1}) [*Morris et al.*, 2001]. Our tracer-based estimates of Ψ agree with geostrophic estimates: 6.7 ± 0.5 Sv at 31°S and 5.0 ± 1.1 Sv at 24°S [*Speer and Zenk*, 1993]. Thus, the $\delta^{18}O$ tracer budget provides a reasonable approximation of the modern Ψ for AABW in the Atlantic.

3.2. LGM $\delta^{18}O$ Budget

[17] The first step in outlining the LGM tracer budget involves defining the domain for AABW in the Atlantic. We use three vertical profiles of $\delta^{18}O$ for this task, one from the Brazil Margin [*Curry and Oppo*, 2005] and two from the Blake Ridge [*Keigwin*, 2004]. Similar to the modern, we can use $\delta^{18}O$ to identify the upper boundary of AABW at the LGM. *Cibicidoides* data from above 2000 m water depth at the Blake Ridge suggest that the northern component end-member had a $\delta^{18}O$ signature of ≤4.0‰ (Figure 2a). Data from below 2000 m water depth at the Brazil Margin indicate that the southern component end-member had a $\delta^{18}O$ signature of ≥4.5‰ (Figure 2c). Given that $\delta^{18}O$ is a conservative tracer, the maximum in $\delta^{18}O_z$ should mark the boundary between northern and southern component waters during the LGM.

[18] Our estimates of $\delta^{18}O_z$ are based on a Monte Carlo approach. We first assign a 1σ calibration error of ±0.18‰ to each LGM data point to account for the scatter observed in regressions between core top foraminiferal $\delta^{18}O$ and predicted $\delta^{18}O$ based on in situ temperature and seawater $\delta^{18}O$ [*Marchal and Curry*, 2008]. This is likely a conservative error given that field-based calibrations reflect not only vital effects, but also the use of nonmodern core tops and spatial and temporal variability in water column properties. We generate 1000 surrogate vertical profiles where every $\delta^{18}O$ value is sampled from a Gaussian distribution with the observed mean value and a standard deviation of 0.18‰. For each profile, we calculate $\delta^{18}O_z$ by fitting a line to data spanning an 800 m water depth range, and vary the center point of the range from 1500 m to 2700 m. The depth spacing of deep cores at the Blake Ridge precludes use of a water depth range less than 800 m.

[19] The maximum $\delta^{18}O_z$ occurs at $\delta^{18}O$ values of 4.4‰ for the *Cibicidoides sp.* data at both the Brazil Margin and the Blake Ridge, suggesting that the upper boundary of AABW in the Atlantic was defined by this value (Figure 9). A similar structure is observed for the *Uvigerina sp.* data at Blake Margin, but with an offset in absolute $\delta^{18}O$ which is likely due to vital effects [*Keigwin*, 2004]. Thus, the basic structure of the LGM water column profiles is resilient to the large scatter induced by a ±0.18‰ calibration error for $\delta^{18}O$. This result strongly suggests there was a water mass boundary near 2 km water depth at the LGM, and that this boundary was defined by a $\delta^{18}O$ of 4.4 ± 0.1‰. The medians of each $\delta^{18}O_z$ distribution overlap at 1σ: (−0.9 ± 0.2) × 10^{-3}, (−1.0 ± 0.3) × 10^{-3}, and (−1.0 ± 0.3) × 10^{-3} ‰/m for Brazil *Cibicidoides*, Blake *Cibicidoides*, and Blake *Uvigerina*, respectively (Table 2). We use an average of all three (Figure 10, top) in our calculation of Ψ/κ for the LGM.

[20] The difference in $\delta^{18}O$ between water entering the South Atlantic and the upper boundary of AABW at 27°S ($\Delta\delta^{18}O$) is the largest source of uncertainty in calculating Ψ/κ for the LGM. Although the upper value is well constrained, there are no $\delta^{18}O$ data below 3000 m water depth at the Brazil Margin. To estimate $\delta^{18}O$ of AABW entering the Atlantic, we extrapolate the linear trend in $\delta^{18}O$ from 2000 to 3000 m water depth to 4500 m, yielding a bottom value of 5.0 ± 0.2‰. In the modern South Atlantic, $\delta^{18}O$ increases linearly all the way to seafloor, supporting our assumption for the LGM. If instead abyssal $\delta^{18}O$ was nearly constant below 3000 m ($\delta^{18}O \sim 4.6$‰), our estimate of Ψ/κ for the LGM would increase.

[21] We calculated $\Delta\delta^{18}O$ as linear regressions between the midpoint of the maximum $\delta^{18}O_z$ (i.e., the water mass boundary) and the bottom of the ocean at 4500 m for each of the 1000 randomly generated profiles. The median $\Delta\delta^{18}O$ is −0.46 ± 0.23‰ (Figure 10, middle), and the $\Delta\delta^{18}O/\delta^{18}O_z$ ratio peaks at 440 ± 230 m (Figure 10, bottom). The LGM $\Delta\delta^{18}O/\delta^{18}O_z$ ratio is statistically indistinguishable from the modern ratio (390 ± 160 m; Table 1). We plot $\Delta\delta^{18}O/\delta^{18}O_z$ instead of $\delta^{18}O_z/\Delta\delta^{18}O$ because division by $\Delta\delta^{18}O$ values close to zero creates infinitely large ratios.

3.3. Modern $\delta^{13}C$ Budget

[22] To evaluate *Pe* for the modern Atlantic it is necessary to calculate $\delta^{13}C_z$ and $\Delta\delta^{13}C$. Our estimates of these parameters are derived from WOCE and Ocean-Atmosphere Carbon Exchange Study (OACES) $\delta^{13}C$ profiles (Figure 11). We estimate the budget for $\delta^{13}C$ = 0.70‰ which approximately follows the $\delta^{18}O$ = 3.08‰ surface. We calculated $\Delta\delta^{13}C$ at 30°S using $\delta^{13}C$ of the isosurface minus $\delta^{13}C$ near the seafloor. Because there were no water column $\delta^{13}C$ data below 4000 m near the Brazil site, data from 45°S to 35°S were used to estimate an abyssal $\delta^{13}C$ value of 0.46‰

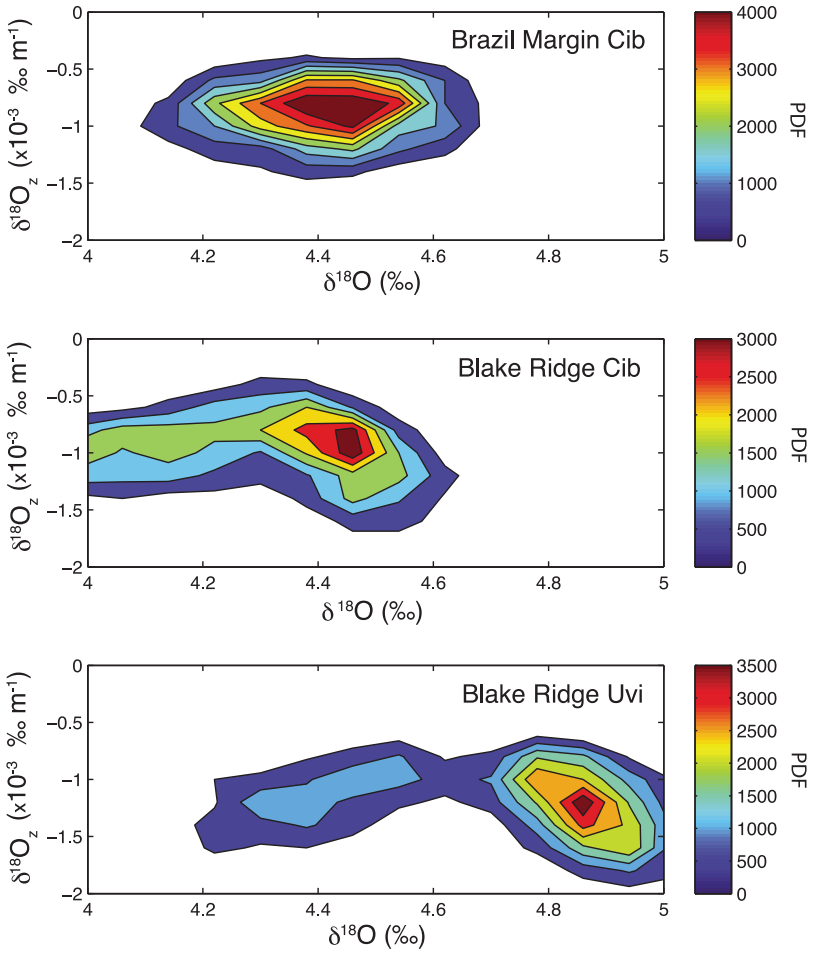

Figure 9. Probability density functions from the Monte Carlo results of $\delta^{18}O_z$ as a function of $\delta^{18}O$ for the LGM data. These contour plots show that the water mass boundary at ~4.4‰ between northern and southern source waters at the LGM is a robust feature of the data even when an error of 0.18‰ is added to each data point. *Cibicidoides sp.* data at (top) the Brazil Margin and (middle) the Blake Ridge is shown with each peak at ~4.4‰. (bottom) *Uvigerina sp.* data at the Blake Ridge and peak at ~4.9‰. The offset in $\delta^{18}O$ between the species is most likely due to vital effects.

Table 2. Parameters for LGM Tracer Budget[a]

	Vertical Gradient[b] ($\times 10^{-4}$‰ m^{-1})	Vertical Difference[c] (‰)	Ratio[d] (m)	Area ($\times 10^{12}$ m^2)	Ψ/κ ($\times 10^{10}$ m)	*Pe*
			$\delta^{18}O$ = 4.4‰			
Brazil (Cib)	−8.7 ± 2.4	−0.46 ± 0.23	530 ± 250	45 ± 9	13 ± 7	
Blake (Cib)	−9.9 ± 3.1					
Blake (Uvi)	−10.2 ± 3.1					
Average	−10.0 ± 1.7	−0.46 ± 0.23	440 ± 230	45 ± 9	16 ± 9	
			$\delta^{13}C$ = 0.6‰			
Brazil (Cib)	10.0 ± 2.0	1.14 ± 0.25	1140 ± 340	45 ± 9	6 ± 2	2.2 ± 1.2
Blake (Cib)	14.0 ± 3.2					
Average	12.0 ± 2.0	1.14 ± 0.25	930 ± 250	45 ± 9	7 ± 3	2.1 ± 1.3

[a]Domain of AABW at LGM spanned from 27°S to 60°N and from the 2000 m isobath to the seafloor, a volume of ~1×10^{17} m^3. For the modern, AABW spans from 27°S to the equator and from 4000 m to the seafloor, a volume of ~5×10^{15} m^3.
[b]Vertical gradients are $\delta^{18}O_z$ and $\delta^{13}C_z$.
[c]Vertical differences are $\Delta\delta^{18}O$ and $\Delta\delta^{13}C$.
[d]Ratios are $\Delta\delta^{18}O/\delta^{18}O_z$ and $\Delta\delta^{13}C/\delta^{13}C_z$.

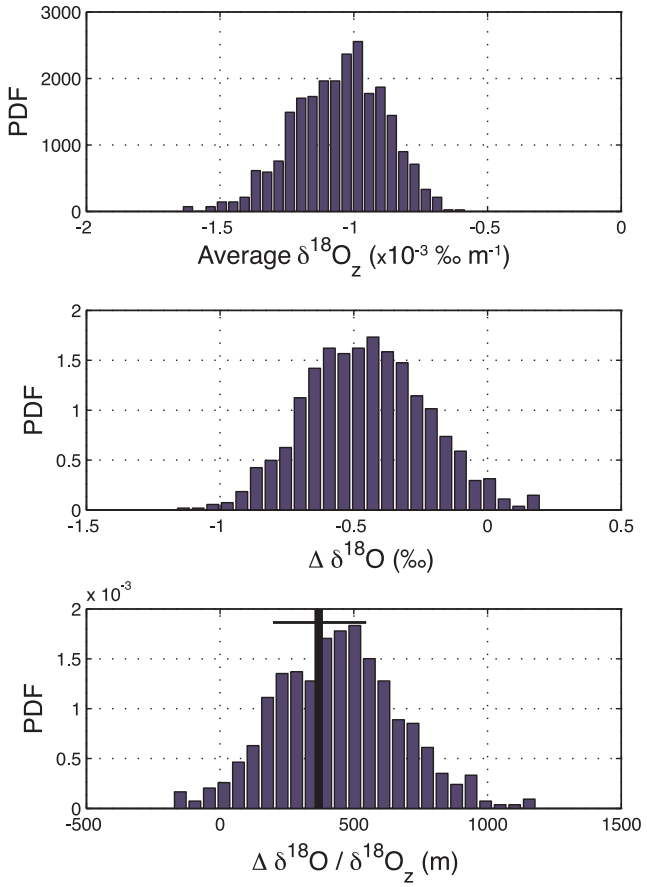

Figure 10. (top) Probability density function of the average $\delta^{18}O_z$ for the three LGM $\delta^{18}O$ profiles. (middle) Probability density function of $\Delta\delta^{18}O$ at the Brazil Margin. (bottom) Probability density function of $\Delta\delta^{18}O/\delta^{18}O_z$ for the LGM data. We plot $\Delta\delta^{18}O/\delta^{18}O_z$ instead of $\delta^{18}O_z/\Delta\delta^{18}O$ because division by $\Delta\delta^{18}O$ values close to zero creates infinitely large ratios. The peak in the $\Delta\delta^{18}O/\delta^{18}O_z$ PDF overlaps with the average of $\Delta\delta^{18}O/\delta^{18}O_z$ for the modern $\delta^{18}O$ surface of 3.08‰ (solid vertical line; 390 ± 160 m).

(water depths >4200 m). Together, these data yield a $\Delta\delta^{13}C$ of 0.24 ± 0.05‰ (Table 1).

[23] We calculated the gradient in $\delta^{13}C$ ($\delta^{13}C_z$) across each isosurface for the latitude bins presented in Figure 11, using data from 300 m above and below the designated $\delta^{13}C$ surface, similar to the water depth range used to calculate $\delta^{18}O_z$ for modern AABW. We estimate a $\delta^{13}C_z$ for the upper "lid" of AABW of (4.8 ± 1.0) × 10^{-4} ‰ m^{-1} (Table 1). The $\delta^{13}C_z$ estimates are largest in the South Atlantic where the presence of nutrient-enriched (^{13}C depleted) AABW is the most obvious. Our estimate of the $\Delta\delta^{13}C/\delta^{13}C_z$ ratio (510 ± 150 m) is within one sigma error of the $\Delta\delta^{18}O/\delta^{18}O_z$ ratio for the modern Atlantic (390 ± 160 m) (Table 1).

3.4. LGM $\delta^{13}C$ Budget

[24] Our constraints for the LGM $\delta^{13}C$ budget come from the *Cibicidoides* $\delta^{13}C$ profiles at the Brazil Margin and Blake Ridge. As with the $\delta^{18}O$ data, we use a Monte Carlo technique to test the robustness of our tracer budget calculation to uncertainty in the $\delta^{13}C$ data. We estimate an RMS error of 0.14‰ for the regression between Holocene *Cibicidoides* $\delta^{13}C$ and $\delta^{13}C$ of dissolved inorganic carbon from *Duplessy et al.* [1984] (Figure 12). This calibration error is likely a maximum estimate, because (1) the sediment cores used in the regression lack good chronological control, meaning that the regression between dissolved inorganic carbon $\delta^{13}C$ and benthic foraminiferal $\delta^{13}C$ includes error associated with the unknown time offset between sediment and hydrographic data, and (2) the hydrographic data used by *Duplessy et al.* [1984] were sparse and required interpolation to match core locations.

[25] Assuming a 0.14‰ uncertainty for individual $\delta^{13}C$ points, we randomly generate 1000 $\delta^{13}C$ profiles from these distributions. We calculate $\delta^{13}C_z$ by fitting a line to data spanning an 800 m water depth range, and vary the center point of the range from 1500 m to 2700 m. Figure 13 shows a 2-D histogram of the vertical $\delta^{13}C$ gradient ($\delta^{13}C_z$) and its corresponding $\delta^{13}C$ for these 1000 profiles. The largest gradient occurs at similar $\delta^{13}C$ values for each site, although the PDF is shifted toward lower $\delta^{13}C$ at the Brazil Margin. The two sites also have similar $\delta^{13}C_z$ values, but the pdf is shifted toward slightly higher $\delta^{13}C_z$ at Blake Ridge. The steeper tracer gradient at Blake Ridge may reflect the greater influence of ^{13}C-enriched northern component water at this latitude. To obtain the area averaged $\delta^{13}C_z$ for our budget, we averaged the $\delta^{13}C_z$ estimates from each location. The resulting values have a wide distribution with a median $\delta^{13}C_z$ of 1.2 × 10^{-3}‰ m^{-1} (Figure 14, top).

[26] The broad histogram of mean $\delta^{13}C_z$ values can be combined with the $\Delta\delta^{13}C$ data from Brazil Margin (defined as before for $\Delta\delta^{18}O$) to calculate the $\Delta\delta^{13}C/\delta^{13}C_z$ ratio. We estimate a $\delta^{13}C$ at 4500 m of −0.8 ± 0.2‰, based on linear extrapolation of the $\delta^{13}C$ trend in shallower water. This value is in good agreement with $\delta^{13}C$ for the abyssal southwest Atlantic [*Ninnemann and Charles*, 2002]. The median of the difference between $\delta^{13}C$ at the seafloor and the top of our control volume ($\Delta\delta^{13}C$) for the LGM is 1.2‰ (Figure 14, middle). In combination with $\delta^{13}C_z$, this yields a median $\Delta\delta^{13}C/\delta^{13}C_z$ of 930 ± 250 m (Figure 14, bottom). Although this distribution overlaps with the distribution of $\Delta\delta^{13}C/\delta^{13}C_z$ for the modern, the agreement is not as good as that between the modern and LGM distributions of $\Delta\delta^{18}O/\delta^{18}O_z$ (Figure 10).

4. Discussion

4.1. Modern Versus LGM Ψ/κ and *Pe*

[27] Our estimates of $\delta^{18}O_z$ and $\Delta\delta^{18}O$ for the LGM yield a $\Delta\delta^{18}O/\delta^{18}O_z$ distribution that overlaps with modern values. However, to calculate Ψ/κ we must also account for the larger surface area over which tracer diffused into and out of AABW during the LGM (see equation (2)). The maximum in $\delta^{18}O_z$ at $\delta^{18}O$ ~ 4.4‰ indicates the upper lid of AABW spanned 27°S to at least 30°N and was located at a water depth of ~2000 m. The $\delta^{13}C$ tracer field suggests that AABW reached 60°N in the Atlantic and encompassed both the western and eastern basins [*Duplessy et al.*, 1988; *Oppo and Lehman*, 1993; *Curry and Oppo*,

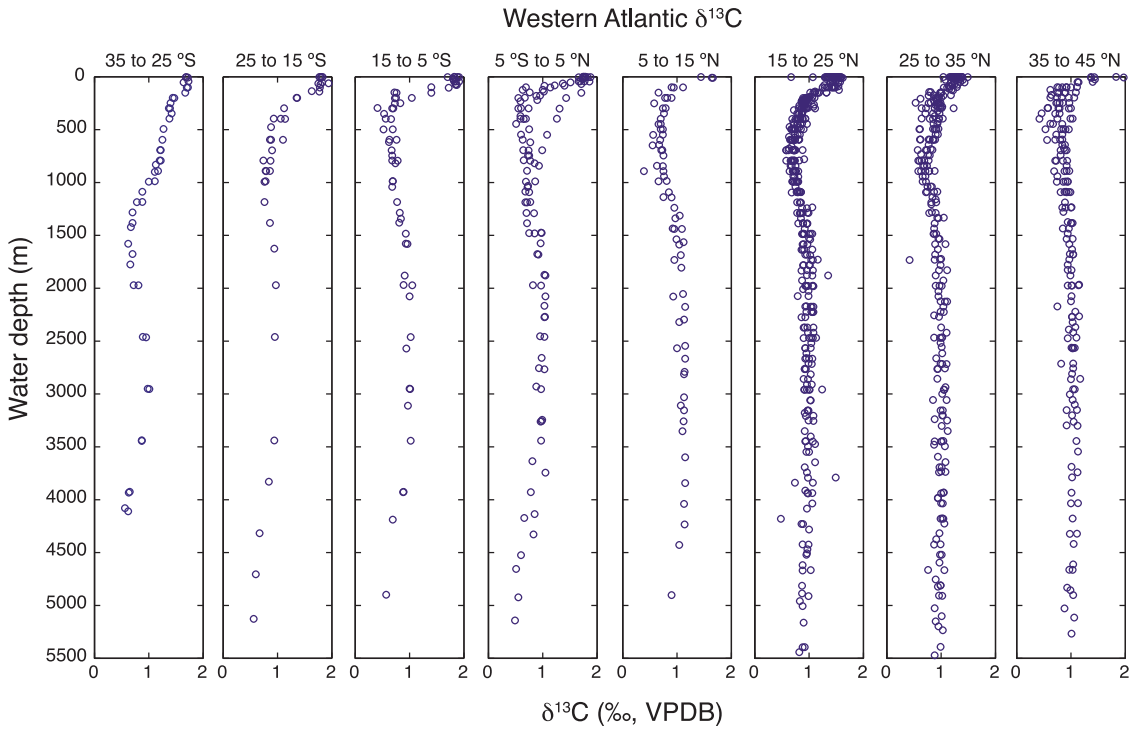

Figure 11. Water column $\delta^{13}C$ of DIC values for the western Atlantic Ocean, partitioned into 10° latitude bins. Data from 35°S to 5°N are from the Ocean Atmosphere Carbon Exchange Study (OACES; http://cdiac3.ornl.gov/las/servlets/dataset) and data from 5°N to 45°N are from World Ocean Circulation Experiment (WOCE) lines AR01, A20, and A22 (http://cchdo.ucsd.edu/atlantic.html). The influence of AABW is most prominent in the South Atlantic, where $\delta^{18}C$ values below 4000 m approach −0.5‰. North of 15°N, the influence of AABW is barely perceptible.

2005]. The area of the horizontal surface in the Atlantic Ocean from 27°S to 60°N along the 2000 m isobath is approximately 4.5×10^{13} m^2 (Table 2). If AABW reached to only 50°N during the LGM, its area would have been 4.3×10^{13} m^2, about 10% lower. By comparison, the area of the upper lid of AABW in the modern Atlantic is $(4.7 \pm 0.5) \times 10^{12}$ m^2. Therefore, the area of AABW was about an order of magnitude larger at the LGM. Accounting for the difference in surface area, we estimate that Ψ/κ was approximately eight times larger at the LGM.

[28] The considerable errors for both our Ψ/κ estimates make it difficult to precisely determine the change in Ψ/κ from LGM to modern. We can, however, estimate the minimum difference between the two climate states. The smallest possible Ψ/κ for the LGM is set by the largest possible $\Delta\delta^{18}O/\delta^{18}O_z$ ratio, or 1200 m (Figure 10, bottom). Using this value yields a minimum Ψ/κ for the LGM of 5.7×10^{10} m. Because the minimum estimate of the LGM Ψ/κ is at least two times the modern value, either the LGM transport was larger than today, the vertical mixing less, or some combination of the two. We explore the likelihood of these scenarios below. Given that the $\Delta\delta^{18}O/\delta^{18}O_z$ histogram also includes values near zero, the upper limit for Ψ/κ during the LGM is unconstrained by the available data.

[29] By adding $\delta^{13}C$ to the tracer budget we can assess how the larger Ψ/κ ratio affected the bulk *Pe* defined in

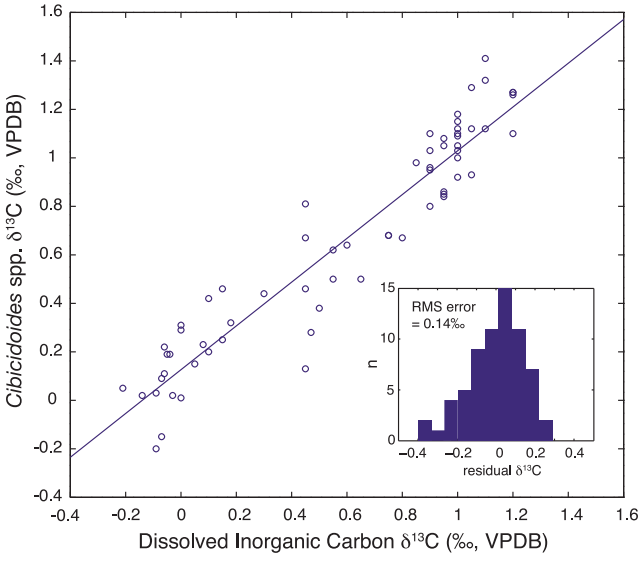

Figure 12. Scatterplot of dissolved inorganic carbon $\delta^{13}C$ versus Holocene *Cibicidoides* $\delta^{13}C$ data from *Duplessy et al.* [1984]. We estimate an RMS error of 0.14‰ for the regression between the two parameters. Inset shows a histogram of residual values (i.e., foraminiferal $\delta^{13}C$ values predicted by the regression minus observed foraminiferal $\delta^{13}C$).

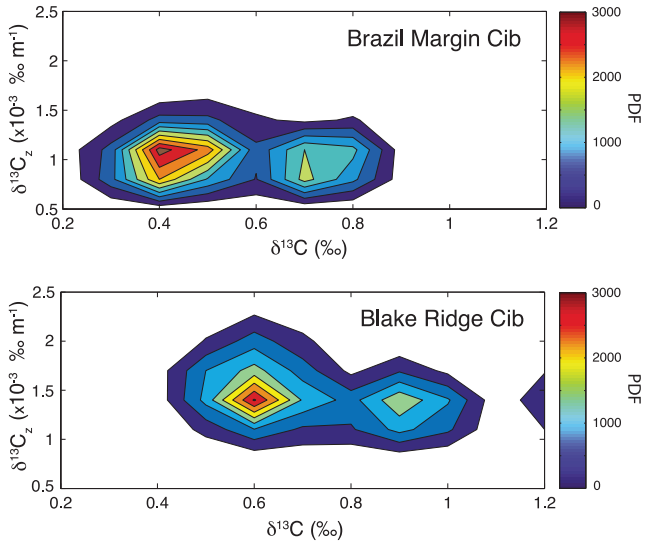

Figure 13. Probability density function of the vertical gradient in $\delta^{13}C$ ($\delta^{13}C_z$) versus $\delta^{13}C$ where the maximum in $\delta^{13}C_z$ occurs. At Brazil Margin, the maximum in $\delta^{13}C_z$ occurs at $\delta^{13}C$ values between 0.3‰ and 0.8‰. At Blake Ridge, the range is from 0.5‰ to 1.0‰. The maximum $\delta^{13}C_z$ values are generally higher at Blake Ridge, with a median of 1.4×10^{-3}‰/m, while at Brazil Margin the median is 1.0×10^{-3}‰/m.

equation (4). One of the long standing issues in paleoceanography is whether the glacial $\delta^{13}C$ tracer field primarily reflects the biological remineralizaton of organic matter or the physical circulation of the ocean. In principle, we should be able to partition the influences of remineralization and circulation on $\delta^{13}C$ using the tracer budget. As outlined in the methods, we can estimate a Peclet number for $\delta^{13}C$ (the ratio of $\delta^{13}C$ transport to $\delta^{13}C$ diffusion) using parameters from the $\delta^{13}C$ profiles ($\Delta\delta^{13}C$ and $\delta^{13}C_z$) and Ψ/κ derived from the $\delta^{18}O$ tracer budget. If $Pe = 1$, then the diffusive and transport fluxes balance, and the remineralization flux is negligible. When $Pe < 1$, the tracer displays nonconservative behavior because remineralization influences the budget. For example, a Pe of 0.5 would indicate that ~50% of the diffusive flux is balanced by remineralization. Pe values above 1 indicate the tracer inventory is out of balance.

[30] Using our estimates of $\delta^{13}C_z$, $\Delta\delta^{13}C$, and the Ψ/κ from the $\delta^{18}O$ budget, we calculate a Pe of 1.3 ± 0.7 for modern AABW (Table 1). The advective flux of $\delta^{13}C$ appears to be largely balanced by the diffusive flux. If this is correct, $\delta^{13}C$ is essentially conservative and it can be used to independently estimate Ψ/κ. Our $\delta^{13}C$-based Ψ/κ estimate of $1.4 \pm 0.4 \times 10^{10}$ m is very similar to the $\delta^{18}O$-dervived value (Table 1). However, at 1σ the minimum Pe also suggests that remineralization may account for up to 40% of the $\delta^{13}C$ sink for the abyssal Atlantic. Our results also includes Pe values >1, which would indicate the tracer inventory is out of balance and that we have not accounted for all of the important fluxes.

[31] For the LGM, our estimates of $\Delta\delta^{18}O/\delta^{18}O_z$ and $\Delta\delta^{13}C/\delta^{13}C_z$ yield a Pe of 2.1 ± 1.3 (Table 2). Similar to the modern, Pe spans a range of values above and below 1. Assuming a $Pe \sim 1$, the $\delta^{13}C$-derived Ψ/κ would be (7.3 ± 2.5) × 10^{10} m, within error of the $\delta^{18}O$-derived value of (16 ± 9) × 10^{10} m. The agreement is not as good as for the modern, however. Overall, the LGM Pe estimates span over a higher range of values, suggesting the LGM budget may be imbalanced. Given that Pe values >1 imply we have not fully accounted for all the fluxes of tracer, it is important to ask where there are likely sources of error in our analysis. In section 4.2 we consider the uncertainties in the tracer balances.

4.2. Sources of Error in the Tracer Budgets

4.2.1. Along Isopycnal Mixing Into the Control Volumes

[32] The full budget for $\delta^{18}O$ outlined in Appendix A includes contributions from mixing both across (κ) and along isopycnal surfaces (κ_{iso}). Our tracer budget includes only cross-isopycnal mixing in the estimate of the Ψ/κ ratio, an acceptable approximation if isolines of $\delta^{18}O$ are parallel

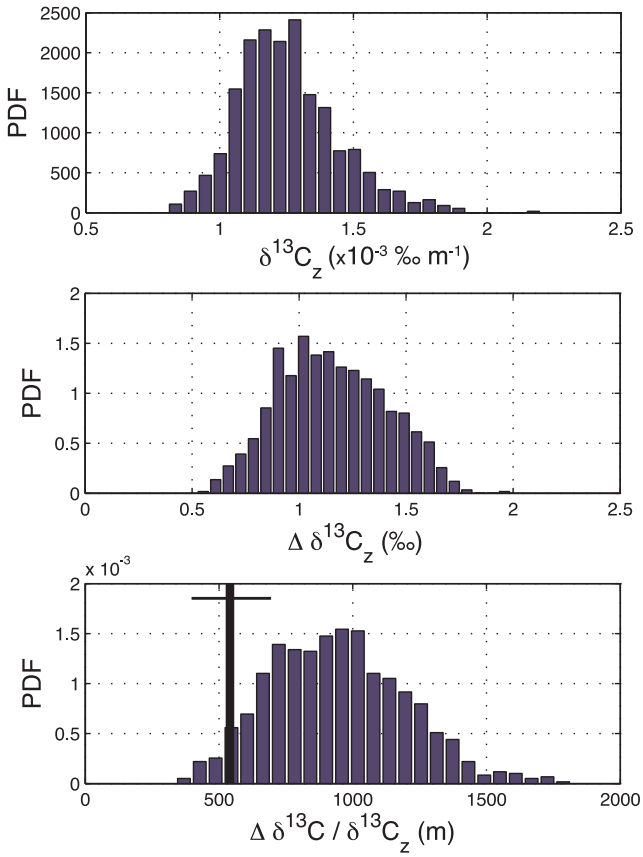

Figure 14. (top) Average LGM $\delta^{13}C_z$ for the Brazil Margin and Blake Ridge from Figure 13. (middle) LGM $\Delta\delta^{13}C$ for the Brazil Margin based on 1000 randomly generated profiles, a calibration error of ±0.14‰, and a value at 4500 m water depth of −0.8‰ (see text). (bottom) Probability density function of $\Delta\delta^{13}C/\delta^{13}C_z$ for the LGM data. The median for the LGM is 930 ± 250 m, larger than that for the modern (510 ± 150 m).

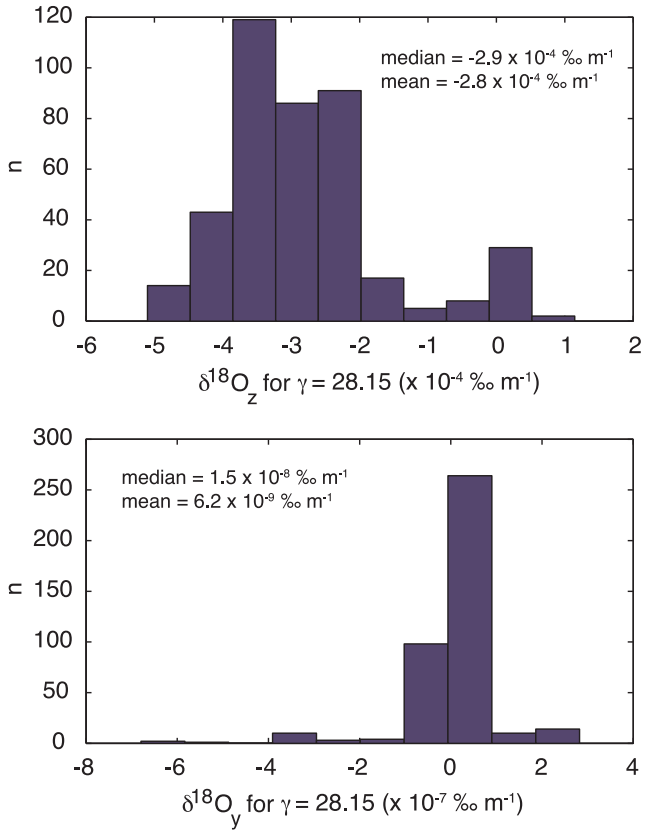

Figure 15. (top) Histogram of the vertical gradient in $\delta^{18}O$ ($\delta^{18}O_z$) across the neutral density surface $\gamma = 28.15$ kg/m^3 in the modern Atlantic. Nearly all of the values are negative, meaning $\delta^{18}O$ increases with depth. The median $\delta^{18}O_z$ is 2.9×10^{-4}‰ m^{-1}. (bottom) Histogram of the along isopycnal gradient in $\delta^{18}O$ ($\delta^{18}O_y$) where $\gamma = 28.15$ kg/m^3. Values are both positive and negative, meaning fluxes are into and out of the control volume. We use the median (1.5×10^{-8}‰ m^{-1}) to yield the largest tracer slope (s_c) for evaluating along versus across isopycnal diffusion of $\delta^{18}O$ (see text).

to lines of constant density. The additional along isopycnal mixing that arises if the isosurfaces are not parallel is negligible only if

$$\kappa \gg \kappa_{iso} |s_c - s_\rho|^2 \quad (5)$$

where s_c is the slope of the tracer surface (s_c = horizontal $\delta^{18}O$ gradient/vertical $\delta^{18}O$ gradient) and s_ρ is the slope of the density surface at the same point. The difference $|s_c - s_\rho|$ is approximately equal to the along isopycnal tracer gradient divided by the vertical tracer gradient. In the modern Atlantic, we define the upper boundary of AABW using the neutral density surface $\gamma \sim 28.15$ kg/m^3 or equivalently the $\delta^{18}O = 3.08$‰ surface. The median $\delta^{18}O_z$ across this surface is -2.9×10^{-4}‰ m^{-1} (Figure 15, top). We estimate $\delta^{18}O_y$ at each grid point using $\delta^{18}O$ values immediately to the north and south (given a grid spacing of 1°, $\delta^{18}O_y$ is calculated over 2° latitude). The median along isopycnal gradient is 1.5×10^{-8}‰ m^{-1} (Figure 15, bottom). Together these yield $|s_c - s_\rho| \approx 5 \times 10^{-5}$. Using equation (5) and typical diffusivities, κ_{iso} = O(1000) m^2/s and κ = O(10^{-4}) m^2/s [*Stammer*, 1998; *Ledwell et al.*, 1998], we find that the along-density diffusion of $\delta^{18}O$ is ~40 times smaller than the cross-density diffusion and can be neglected for the modern case.

[33] Given that we have no direct constraints on the abyssal density field in the geologic past, we can only speculate about along isopycnal mixing of $\delta^{18}O$ and $\delta^{13}C$ at the LGM. We assume that isopyncals in the deep Atlantic were nearly horizontal north of 30°S, as they are today (Figure 4). Available stable isotope data for the LGM suggest the $\delta^{18}O$ isolines were nearly horizontal as well. The LGM boundary between southern and northern component waters occurred at 4.4 ± 0.1‰, or 2000 ± 200 m water depth at the Brazil Margin (~30°S) and Blake Ridge (~30°N). Today, $\delta^{18}O$ surfaces that bound the upper lid of AABW (3.05–3.10‰) vary by up to 1 km over the same latitude range (Figure 5). It is therefore plausible that both s_c and s_ρ were small at the LGM and along isopycnal diffusion of $\delta^{18}O$ played a negligible role in the tracer budget. For both today and the LGM, along-isopycnal diffusion of $\delta^{18}O$ into AABW appears to be important only in the Southern Ocean, where AABW comes to the surface and tracer and density slopes become very steep. The Southern Ocean, however, is south of our tracer budget domain.

[34] While along isopycnal mixing is not important for $\delta^{18}O$, it may be an issue for $\delta^{13}C$ because it has a different spatial distribution. Using $\delta^{13}C$ values at the approximate depths of the neutral density surface $\gamma \sim 28.15$ in the modern ocean, we estimate a $\delta^{13}C_z$ of ~5×10^{-4}‰ m^{-1} (Table 1) and an along-isopycnal $\delta^{13}C$ gradient of ~5×10^{-8}‰ m^{-1} (a 0.2‰ increase over 60° latitude; Figure 16). Together, this yields $|s_c - s_\rho| \approx 1 \times 10^{-4}$. These values

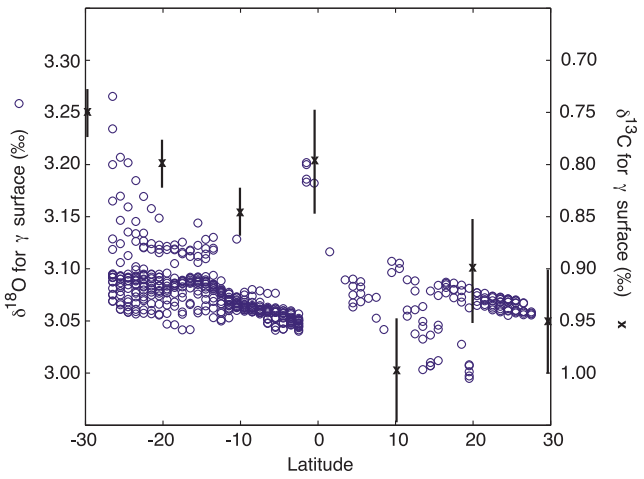

Figure 16. Plot of $\delta^{18}O$ (circles) and $\delta^{13}C$ (crosses) versus latitude along the neutral density surface $\gamma = 28.15$. To estimate the $\delta^{13}C$ values, we determined the approximate depth of $\gamma = 28.15$ in each latitude bin of Figure 11 and used the $\delta^{13}C$ at that water depth. We estimate an along isopycnal gradient of 5×10^{-8}‰ m^{-1} for $\delta^{13}C$, approximately twice the horizontal gradient for $\delta^{18}O$.

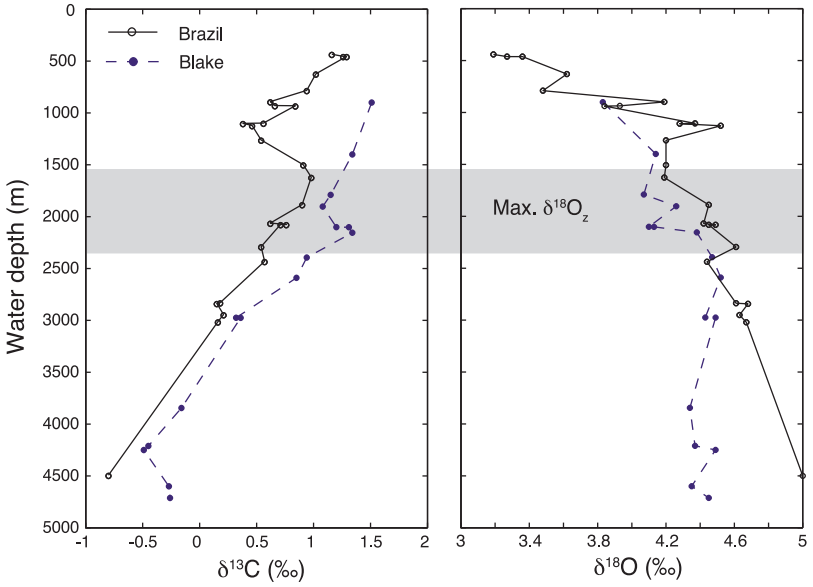

Figure 17. (left) Water depth versus benthic foraminiferal $\delta^{13}C$ at the LGM for the Brazil Margin (solid line) [*Curry and Oppo*, 2005] and Blake Ridge (dashed blue) [*Keigwin*, 2004]. At the Brazil Margin, we estimated $\delta^{13}C$ below 3000 m by linear extrapolation of the 2000–3000 m trend to 4500 m. The resulting value of −0.8‰ is consistent with values of −0.8‰ from the southeast Atlantic [*Ninnemann and Charles*, 2002]. The maximum vertical gradient in $\delta^{13}C$ ($\delta^{13}C_z$) occurs between 2500 m and 3000 m water depth. (right) Water depth versus benthic foraminiferal $\delta^{18}O$ at the LGM for the Brazil Margin (solid line) and Blake Ridge (dashed line). At the Brazil Margin, we estimated $\delta^{18}O$ below 3000 m by linear extrapolation of the 2000–3000 m trend to 4500 m. A lower $\delta^{18}O$ value at 4500 m decreases $\Delta\delta^{18}O$ and therefore increases Ψ/κ for the LGM. The maximum vertical gradient in $\delta^{18}O$ ($\delta^{18}O_z$) occurs at ~2000 m water depth (horizontal gray bar).

suggest the along-isopycnal diffusion of $\delta^{13}C$ is ~10% of the diapycnal diffusion in the modern Atlantic. Therefore, along-isopycnal mixing seems to be a minor term in the modern $\delta^{13}C$ tracer budget.

[35] Along isopycnal mixing may play a more significant role in the budget for $\delta^{13}C$ at the LGM. The contrast in $\delta^{13}C$ between northern and southern component waters at the LGM (~2.5‰) was more than twice the $\delta^{18}O$ contrast (~1‰) (Figure 17). As a result, along isopycnal mixing likely played a more important role in the tracer budget for $\delta^{13}C$ than $\delta^{18}O$. Indeed, our estimate of *Pe* for the LGM includes values greater than 1. If in reality *Pe* was this large, it would indicate that we underestimated the ^{13}C flux into our control volume. A likely candidate for this missing flux is along isopycnal mixing.

4.2.2. Other Possible Errors in the $\delta^{18}O$ Budget

[36] In the preceding discussion, we referred to $\delta^{18}O$ as a conservative tracer. Because benthic foraminiferal $\delta^{18}O$ reflects in situ rather than potential temperature, it is not strictly conservative. The effect of compressive heating on the Ψ/κ estimates is small, however. In the case of the modern AABW, the pressure effect makes water entering the South Atlantic at 4500 m about 0.1°C warmer than water leaving the South Atlantic at 3500 m. Given a $\delta^{18}O$-T relationship of 0.2‰ per °C, the implication is that the deep $\delta^{18}O$ value is reduced by about 0.02‰. If we adjust $\Delta\delta^{18}O$ for this effect, the modern Ψ/κ estimate decreases by 11%. During the LGM, the correction is larger (0.05‰) because the upper boundary of southern component water was near 2000 m water depth. If we increase the LGM $\Delta\delta^{18}O$ by 0.05‰, Ψ/κ decreases by 13%. While significant, the $\Delta\delta^{18}O$ adjustments do not change our result that Ψ/κ was larger at the LGM.

[37] Our LGM budget is based on three vertical $\delta^{18}O$ profiles, one from the Brazil Margin and two from the Blake Ridge. This is a small data set for analyzing the LGM southern source water mass, especially given that much more $\delta^{13}C$ data has been used to make tracer maps like Figure 1. We use these locations because they are the only LGM $\delta^{18}O$ profiles in the Atlantic which meet the following criteria: (1) the cores used to create each depth profile are from tightly constrained geographic regions, (2) the sedimentation rates in the cores are high (generally >5 cm kyr^{-1}), (3) the core depths span most of the water depth range relevant to AABW, and (4) the stable isotope data used to create each profile was run within an individual laboratory. Running in a single laboratory is particularly important for creating high-fidelity profiles of $\delta^{18}O$ versus water depth. Interlaboratory offsets of ~0.3‰ for benthic $\delta^{18}O$ [*Ostermann and Curry*, 2000; *Hodell et al.*, 2003] are similar to the total range of $\delta^{18}O$ variability in the abyssal Atlantic during the LGM. As a result, it is very difficult to make coherent maps of benthic $\delta^{18}O$ similar to those that exist for $\delta^{13}C$ [*Zahn and Mix*, 1991]. As laboratory intercalibration improves and additional depth transects from high sedimentation rate sites become available, it will be

possible to test whether the few available profiles provide a reliable picture of the abyssal Atlantic $\delta^{18}O$ tracer field at the LGM.

4.3. Comparing the $\delta^{13}C$ and $\delta^{18}O$ Results

[38] The discussion above makes two important points. First, the ratio of Ψ/κ at the LGM was approximately eight times larger than it is today. Second, the difference in *Pe* values was not nearly as large, though uncertainties in the $\delta^{13}C$ budget make it difficult to quantify the ratio of $\delta^{13}C$ transport to tracer diffusion. Given this analysis, it is instructive to consider the LGM stable isotope profiles (Figure 17). At 27°S, $\delta^{18}O$ increases monotonically below the boundary between northern and southern source waters. This shape is to be expected if dense, cold, and salty waters are transported into the Brazil Basin at the LGM. By the time this water mass reaches the Blake Ridge in the Northern Hemisphere vertical diffusion has worked to homogenize the vertical $\delta^{18}O$ profile.

[39] The structure of the $\delta^{13}C$ profiles is fundamentally different than those for $\delta^{18}O$. First, the slope of the $\delta^{13}C$ profiles is opposite that for the $\delta^{18}O$ profiles, because the southern end-member has lower $\delta^{13}C$ than the northern end-member. Second, the slope of the Blake and Brazil profiles is essentially identical (Figure 17). An extra flux of low $\delta^{13}C$ works against the tendency of vertical mixing to homogenize the profile. A likely candidate for this extra flux is biological remineralization. By adding isotopically depleted DIC to the water mass continuously along its flow path, this nonconservative term has the opposite effect than diffusive mixing of isotopically enriched northern source water. That these two processes would leave the $\delta^{13}C$ profiles roughly parallel seems like a coincidence as there is no a priori reason that mixing and remineralization should be of nearly the same size.

4.4. The Combined Roles of Transport and Vertical Mixing

[40] Our analysis of the available LGM $\delta^{18}O$ profiles in the Atlantic shows that Ψ/κ for AABW was larger than today. Similar to the local balance between upwelling and diffusion postulated for the modern North Pacific by W. Munk (his "z*" is analogous to our Ψ/κ) [*Munk*, 1966], a conservative tracer can tell you the ratio of advection to diffusion, but it cannot constrain the two independently. However, we speculate that higher Ψ/κ during the LGM was due to reduced mixing between northern and southern component waters, associated with movement of this water mass boundary away from the seafloor. Today, the upper boundary of AABW sits near 4 km water depth, whereas at the LGM it was at approximately 2 km. In the modern ocean, vertical diffusivities decrease away from bottom topography [*Kunze et al.*, 2006]. Averaged over the Atlantic, vertical mixing is approximately three times lower above 4 km water depth than below [*Ganachaud and Wunsch*, 2000]. In the Brazil Basin, vertical diffusivities over rough topography are an order of magnitude lower at 2 km than at the seafloor [*Polzin et al.*, 1997]. Reduced mixing due to upward migration of the water mass boundary at the LGM is therefore consistent with the vertical profile of κ in the modern ocean, in both sign and magnitude. Our budget results suggest that reduced vertical mixing across the upper boundary of AABW may play a primary role in setting the Atlantic $\delta^{18}O$ tracer field during the LGM. Although we cannot rule out an increase in Ψ, our point is that such an increase is not necessary to explain the tracer distribution in the abyssal Atlantic.

[41] In contrast to our mixing-based interpretation of the $\delta^{18}O$ profiles, the large vertical gradient in $\delta^{13}C$ at the LGM has been interpreted in terms of water mass transport alone [*Duplessy et al.*, 1988; *Curry and Oppo*, 2005]. *Curry and Oppo* [2005] argued that steep gradients in $\delta^{13}C$ are likely maintained by robust deep water flow, if vertical mixing was similar to or greater than today. If the increase in Ψ/κ during the LGM was entirely a function of transport, it would imply that Ψ increased by a factor of 8, a highly unlikely scenario. If instead we use the minimum Ψ/κ for the LGM, it would require a factor of 2 increase in transport. Although more feasible, this would also be a large change in the rate of AABW formation. By comparison, a factor of 2–8 reduction in vertical mixing is reasonable considering the profile of κ in the modern ocean. In reality, both vertical mixing and transport likely changed, but we believe that most of the increase in Ψ/κ at the LGM was due to decreased vertical mixing.

[42] It has been suggested that oceanic vertical mixing was enhanced at the LGM, due in part to exposure of continental shelves and greater tidal dissipation in the deep sea [*Wunsch*, 2003]. If tidal dissipation was confined primarily to water depths below 2 km, however, its effect on mixing across the upper boundary of AABW would have been minimal. Rather than speculate on how κ changed in the past, our scenario calls on the variability in κ with depth in the ocean. The overall shape of this profile must be similar in alternative circulation scenarios, due simply to the presence of rough topography at the bottom of the ocean.

[43] Our constraints on Ψ/κ have implications for the residence time of AABW in the Atlantic. The ~2 km depth of the boundary between southern and northern component waters indicates the volume of AABW in the LGM Atlantic was very large. Assuming that AABW spanned from 27°S to 60°N and across the width of the Atlantic, we estimate its volume was $(1 \pm 0.2) \times 10^{17}$ m^3. For the modern $\delta^{18}O$ surface = 3.08‰, the approximate volume of AABW is $(4 \pm 0.4) \times 10^{15}$ m^3, ~20 times lower than our LGM estimate. If transport during the LGM was similar to the modern value, the residence time would have increased 20 times. If transport was twice that of today, the residence time for AABW would have increased by an order of magnitude. A greater residence time for AABW is consistent with glacial reconstructions of highly depleted radiocarbon values [*Keigwin*, 2004; *Robinson et al.*, 2005] and low Pa/Th ratios in the abyssal North Atlantic [*Gherardi et al.*, 2009].

[44] While our analysis of the $\delta^{18}O$ tracer budget places new quantitative constraints on the LGM Ψ/κ ratio, we would also like to place the results in the context of glacial-interglacial CO_2 variability. The Harvardton Bears box models highlighted the interdependence of nutrient utilization in the Southern Ocean and deep overturning rate in setting atmospheric pCO_2 [*Knox and McElroy*, 1984;

Sarmiento and Toggweiler, 1984; *Siegenthaler and Wenk*, 1984]. Less vigorous circulation and lower preformed nutrient concentrations for southern source deep water both work to lower atmospheric carbon dioxide levels. *Toggweiler* [1999] refined the Havardton Bears by parsing the deep ocean's role into overturning rate and the efficiency of mixing between southern and northern component deep waters. Slower overturning works to lower pCO_2, but carbon and nutrients are brought into contact with the atmosphere if the two deep waters mix efficiently because northern component waters flow back to the North Atlantic via the shallow circulation (in his model at least). Reducing mixing between the deep water masses makes the southern cell a more efficient carbon trap. A lower κ allows for smaller changes in overturning strength and/or nutrient utilization to produce the same lowering of atmospheric pCO_2. In this sense, the results from our $\delta^{18}O$ budget may provide an important clue as to how the glacial deep ocean was involved in lowering atmospheric carbon dioxide levels.

5. Conclusions

[45] The $\delta^{18}O$ of benthic foraminifera in the deep Atlantic show the presence of a water mass boundary at a depth of 2 km during the LGM, defined by a $\delta^{18}O$ value of approximately 4.4‰. The boundary appears to outline the spatial domain of AABW and allows for the creation of a conservative tracer budget based on $\delta^{18}O$. Our approach accounts for transport of $\delta^{18}O$ into the South Atlantic and vertical mixing of $\delta^{18}O$ across the upper boundary of AABW. The $\delta^{18}O$ budget yields reasonable estimates of AABW flow for the modern, giving us confidence that the budget captures the key factors that influence $\delta^{18}O$ in the ocean interior, namely tracer transport and tracer diffusion. For the LGM, we find that the ratio of transport to vertical mixing (Ψ/κ) was at least twice as large as today. Either the transport was greater, the vertical mixing less, or some combination of these two factors. We suggest that the increase in Ψ/κ is most easily explained by reduced vertical mixing. Today, the water mass boundary between northern and southern component waters is located at approximately 4000 m water depth, whereas at the LGM the boundary was near 2000 m. The decrease in vertical mixing over this water depth range in the modern Atlantic (3–10 times) [*Polzin et al.*, 1997; *Ganachaud and Wunsch*, 2000] is broadly consistent with the implied decrease during the LGM.

[46] Box-model experiments invoke limited AABW ventilation and vertical mixing to sequester atmospheric carbon dioxide during the LGM [*Toggweiler*, 1999]. In this scenario, reduced exchange between abyssal and deep water promotes the accumulation of respired CO_2. If reduced vertical mixing at the upper lid of AABW sequestered significant quantities of carbon during glacial times, it should be observed outside the Atlantic Ocean as well. Preliminary $\delta^{18}O$ evidence from the Indian [*Kallel et al.*, 1988] and Pacific [*Herguera et al.*, 1992] show an apparent water mass boundary at 2 km water depth, suggesting the vertical diffusivity may have been reduced on global basis. Sequestration in the abyssal ocean during glacial times also requires minimal leakage of carbon dioxide from the Southern Ocean to the atmosphere. Sea-ice coverage and stratification are other key factors that control Southern Ocean outgassing, yet there is little agreement on how the processes change on glacial-interglacial timescales [*Sigman and Boyle*, 2000; *Keeling and Stephens*, 2001].

[47] Our approach demonstrates that the abyssal Ψ/κ ratio can be constrained using a simple tracer budget and traditional oxygen stable isotope data. Because transport and vertical mixing also influence $\delta^{13}C$, it is likely that the strong $\delta^{13}C$ gradient in the glacial Atlantic was driven in part by reduced mixing between northern and southern component waters. The $\delta^{13}C$ data also suggest that remineralization may influence the evolution of the $\delta^{13}C$ profiles from south to north. In theory, we can combine the $\delta^{13}C$ and $\delta^{18}O$ data to quantify the relative influence of transport, mixing, and remineralization in the abyssal Atlantic. Understanding these parameters is key to understanding the ocean's role in glacial-interglacial CO_2 cycles, and will be a priority for future refinements to the tracer budget approach. In addition, it will be essential to construct new high-fidelity profiles of $\delta^{13}C$ and $\delta^{18}O$ to test whether the results we present here are representative of the Atlantic basin as a whole.

Appendix A: Derivation of the Zonally Averaged Tracer Equation

[48] The evolution of the concentration of a generic tracer c released into the ocean is governed by the advection-diffusion equation,

$$\frac{\partial c}{\partial t} + \left(\mathbf{u} + \mathbf{u}_{eddy}\right) \cdot \nabla c = \nabla \cdot \left(K_{iso} \nabla_{//} c\right) + \nabla \cdot (\kappa \nabla c) + \frac{\partial F_{air-sea}}{\partial z} + J \tag{A1}$$

where t is time, ∇c is the three dimensional tracer gradient, and $\nabla_{//} c$ is the along density surface tracer gradient. This equation describes the evolution of c averaged over the space and timescales characteristic of ocean turbulence, that is, O(100 km) and O(1 week). At these large scales the tracer is advected by the averaged ocean circulation $\mathbf{u}$ and by an eddy-driven circulation $\mathbf{u}_{eddy}$: turbulent eddies result from instabilities of the mean ocean currents and their interactions produce a velocity equivalent to the Stokes drift resulting from surface gravity waves [*Plumb and Ferrari*, 2005]. In addition to a velocity, turbulent eddies drive diffusion of tracers along density surfaces, represented by an isopycnal eddy diffusivity κ_{iso}, and diffusion across density surfaces, represented by the diapycnal diffusivity κ. In the abyssal ocean, the isopycnal diffusivity is typically 7–8 orders of magnitude larger than the diapycnal diffusivity (10^3 m^2/s versus 10^{-4} m^2/s), because eddy fluxes are directed primarily along density surfaces. $F_{air-sea}$ is the flux of tracer at the ocean surface and J includes any interior sources and sinks of nonconservative tracers. The tracer equation must be supplemented by boundary conditions. For the tracers considered in this paper the tracer flux across the solid boundaries is zero; the surface flux is represented explicitly by the $F_{air-sea}$ term. Knowledge of a tracer concentration c, be it $\delta^{18}O$ or $\delta^{13}C$, is generally not sufficient to infer the full

ocean velocity field. But it can be used to infer some bulk properties of the ocean circulation, like the zonally averaged overturning.

[49] We can write an expression for the overturning circulation as a function of latitude and tracer concentration, much alike oceanographers do when they compute the overturning circulation as a function of latitude and density [*Andrews*, 1983; *Nurser and Lee*, 2004]. Consider a zonal slice of the ocean at a fixed latitude y, that is an $x - z$ section through the ocean. We define $A(y, C, t)$ as the area of that section below a certain tracer concentration value C and we assume that the tracer is increasing toward the surface (otherwise the inequalities must be reversed),

$$A(y, C, t) = \iint_{c \le C} \mathrm{d}x\mathrm{d}z \tag{A2}$$

The area $A(y, C, t)$ can be changed either by horizontal advection of water with tracer concentration larger than C, or by nonconservative processes like diffusion, air-sea fluxes or interior sources and sinks,

$$\frac{\partial A}{\partial t} = -\frac{\partial}{\partial y}\iint_{c \le C}\left(v + v_{eddy}\right)\mathrm{d}x\mathrm{d}z - \frac{\partial}{\partial c}\iint_{c \le C}\left[\nabla \cdot \left(K_{iso}\nabla_{//}c\right) + \nabla \cdot (\kappa \nabla c) + \frac{\partial F_{air-sea}}{\partial z} + J\right]\mathrm{d}x\mathrm{d}z \tag{A3}$$

and v and v_{eddy} are the meridional velocity and eddy-induced velocity. Equation (A3) can be simplified if we integrate between any latitude y and the northern or southern continental boundaries and assume steady state,

$$\Psi(y, c) = \frac{\partial}{\partial c}\iiint_{c \le C}\left[\nabla \cdot \left(K_{iso}\nabla_{//}c\right) + \nabla \cdot (\kappa \nabla c) + \frac{\partial F_{air-sea}}{\partial z} + J\right]\mathrm{d}x\mathrm{d}y\mathrm{d}z \tag{A4}$$

where $\Psi(y, C)$ represents the mass meridional transport across the latitude y,

$$\Psi(y, c) = \iint_{c \le C}\left(v + v_{\mathrm{eddy}}\right)\mathrm{d}x\mathrm{d}z \tag{A5}$$

In deriving (A4), we assumed that $\Psi(y, C)$ vanishes at the southern boundary around Antarctica.

[50] Integrating between the surface defined by the C contour and the ocean bottom, we obtain the fundamental equation for our analysis,

$$\int \Psi(y, c)\mathrm{d}c \approx \iint_{c=C} K_{iso}\nabla_{//}c \cdot \mathbf{n}\,\mathrm{d}S + \iint_{c=C} \kappa \nabla c \cdot \mathbf{n}\,\mathrm{d}S + \iint_{c=C} F_{air-sea}\,\mathrm{d}x\mathrm{d}y + \iiint_{c \le C} J\,\mathrm{d}x\mathrm{d}y\mathrm{d}z \tag{A6}$$

where $\mathbf{n}$ is unit vector normal to the bounding surface S, defined by the C contour. The equation can be further simplified because, in the ocean, horizontal tracer gradients are many orders of magnitude smaller than vertical gradients, that is, surfaces of constant tracer concentration are approximately flat. Expanding equation (A6) in the limit of small tracer slopes, one obtains,

$$\int \Psi(y, c)\mathrm{d}c \approx \iint_{c=C} K_{iso}\left|s_c - s_\rho\right|^2 \frac{\partial c}{\partial z}\mathrm{d}x\mathrm{d}y + \iint_{c=C} \kappa \frac{\partial c}{\partial z}\mathrm{d}x\mathrm{d}y + \iint_{c=C} F_{air-sea}\,\mathrm{d}x\mathrm{d}y + \iiint_{c \le C} J\,\mathrm{d}x\mathrm{d}y\mathrm{d}z \tag{A7}$$

where s_c is the slope of the tracer surface and s_ρ is the slope of the density surface at the same point. Mixing of tracer across the C contour is achieved both by along- and across-density diffusion. Diapycnal diffusion dominates if

$$\kappa \gg K_{iso}\left|s_c - s_\rho\right|^2 \tag{A8}$$

For the conservative tracer $\delta^{18}\mathrm{O}$, the $s_c - s_\rho$ term is very small, as shown in the paper, and isopycnal mixing can be ignored. The situation is not as clear for $\delta^{13}\mathrm{C}$.

[51] Consider now the circulation associated with AABW, that is, a circulation that does not outcrop at latitudes north of 60°S. Then the integral (A7) for latitudes north of 60°S reduces to,

$$\int \Psi(y, c)\mathrm{d}c = \iint_{c=C} K_{iso}\left|s_c - s_\rho\right|^2 \frac{\partial c}{\partial z}\mathrm{d}x\mathrm{d}y + \iint_{c=C} \kappa \frac{\partial \mathrm{c}}{\partial z}\mathrm{d}x\mathrm{d}y + \iiint_{c \le C} J\,\mathrm{d}x\mathrm{d}y\mathrm{d}z \tag{A9}$$

For conservative tracers $J = 0$ and the equation has a simple interpretation. The left-hand side of (A9) represents the tracer transport across a latitude y, $\Psi\Delta C$. Tracer transport can only be achieved for $\Delta\mathrm{C} \neq 0$, that is, if the tracer concentration going north is different from the concentration returning south. In order for the tracer concentration to change as it goes around the overturning loop, there must be diffusion of tracer from above, the term in the right-hand side of (A9). At the order of magnitude level, equation (A9) states,

$$\Psi(y, C)\Delta C \propto \kappa \frac{\partial \mathrm{C}}{\partial \mathrm{z}} A \tag{A10}$$

where A is the horizontal area span by the tracer surface C north of y. We dropped the along-density surface diffusion term, because in the region of interest diapycnal diffusion dominates (see section 4). The simple balance (A10) can be compared with the expression derived by W. Munk in the famous paper "Abyssal Recipes" [*Munk*, 1966],

$$w\Delta C \propto \kappa \frac{\partial \mathrm{C}}{\partial \mathrm{z}} \tag{A11}$$

This budget is consistent with (A10) if vertical upwelling is uniform and can be estimated as Ψ/A, that is, the mass flux across the surface A. However, our approach shows that the budget is not local. The balance is between lateral transports of tracer and global vertical fluxes, not between local vertical upwelling and local vertical fluxes.

[52] The budget described by equation (A9) includes tracer transport into and out of the deep South Atlantic. However, our tracer domain is specifically limited to water flowing into the South Atlantic. For the modern climate, we define this domain using the depth of the maximum overturning stream function, which corresponds to the neutral density surface γ = 28.15 kg/m^3 [*Lumpkin and Speer*, 2007] and it is well tracked by a maximum in salinity vertical gradient (Figure 4). Paleoceanographic proxies are too sparse to fully evaluate the terms in (A9). We therefore make some simplifying assumptions about the vertical structure of Ψ and *C*. We assume *C* has a linear vertical gradient within the volume considered, that is,

$$\frac{\partial C}{\partial z} = \frac{\Delta C}{D} \tag{A12}$$

where *D* is the thickness of AABW. The stream function is instead assumed to be quadratic in *z*:

$$\Psi(z) = -\Psi \frac{z(z-2D)}{D^2} \tag{A13}$$

where Ψ is the magnitude of the stream function (and hence of the transport) at the top of AABW and the ocean bottom is set at $z = 0$. This is the simplest vertical structure that gives a northward flow of AABW and a southward flow of NADW. Plugging these expressions in the first integral of equation (A9), we obtain,

$$\frac{2}{3}\Psi \Delta C \approx \kappa \frac{\partial C}{\partial z} A \tag{A14}$$

References

Andrews, D. G. (1983), A finite-amplitude Eliassen-Palm theorem in isentropic coordinates, *J. Atmos. Sci.*, *40*, 1877–1883, doi:10.1175/1520-0469(1983)040<1877:AFAEPT>2.0.CO;2.

Boyle, E. A., and L. D. Keigwin (1982), Deep circulation of the North Atlantic over the last 200,000 years: Geochemical evidence, *Science*, *218*(4574), 784–787, doi:10.1126/science.218.4574.784.

Broecker, W. S. (1982), Ocean chemistry during glacial time, *Geochim. Cosmochim. Acta*, *46*(10), 1689–1705, doi:10.1016/0016-7037(82)90110-7.

Curry, W. B., and G. P. Lohmann (1982), Carbon isotopic changes in benthic foraminifera from the western South Atlantic: Reconstruction of glacial abyssal circulation patterns, *Quat. Res.*, *18*(2), 218–235, doi:10.1016/0033-5894(82)90071-0.

Curry, W. B., and D. W. Oppo (2005), Glacial water mass geometry and the distribution of δ^{13}C of ΣCO_2 in the western Atlantic Ocean, *Paleoceanography*, *20*, PA1017, doi:10.1029/2004PA001021.

Duplessy, J. C., N. J. Shackleton, R. K. Matthews, W. Prell, W. F. Ruddiman, M. Caralp, and C. H. Hendy (1984), ^{13}C Record of benthic foraminifera in the last interglacial ocean: Implications for the carbon cycle and the global deep water circulation, *Quat. Res.*, *21*(2), 225–243, doi:10.1016/0033-5894(84)90099-1.

Duplessy, J. C., N. J. Shackleton, R. G. Fairbanks, L. Labeyrie, D. Oppo, and N. Kallel (1988), Deepwater source variations during the last climatic cycle and their impact on the global deepwater circulation, *Paleoceanography*, *3*(3), 343–360, doi:10.1029/PA003i003p00343.

Ganachaud, A., and C. Wunsch (2000), Improved estimates of global ocean circulation, heat transport and mixing from hydrographic data, *Nature*, *408*(6811), 453–457, doi:10.1038/35044048.

Gebbie, G., and P. Huybers (2006), Meridional circulation during the Last Glacial Maximum explored through a combination of South Atlantic δ^{18}O observations and a geostrophic inverse model, *Geochem. Geophys. Geosyst.*, *7*, Q11N07, doi:10.1029/2006GC001383.

Gherardi, J. M., L. Labeyrie, S. Nave, R. Francois, J. F. McManus, and E. Cortijo (2009), Glacial-interglacial circulation changes inferred from ^{231}Pa/^{230}Th sedimentary record in the North Atlantic region, *Paleoceanography*, *24*, PA2204, doi:10.1029/2008PA001696.

Gouretski, V., and V. Koltermann (2004), WOCE Global Hydrographic Climatology, *Ber. Bundesamtes Seeschifffahrt Hydrogr. 35*, 52 pp., Bundesamtes für Seeschiffahrt und Hydrogr., Hamburg, Germany.

Herguera, J. C., E. Jansen, and W. H. Berger (1992), Evidence for a bathyal front at 2000-M water depth in the glacial Pacific, based on a depth transect on Ontong Java Plateau, *Paleoceanography*, *7*(3), 273–288, doi:10.1029/92PA00869.

Hodell, D. A., C. D. Charles, J. H. Curtis, P. Graham Mortyn, U. S. Ninnemann, and K. A. Venz (2003), Data Report: Oxygen Isotope Stratigraphy of Leg 177 Sites 1088, 1089, 1090, 1093, and 1094, *Proc. Ocean Drill. Program Sci. Results*, *177*, 1–26.

Kallel, N., L. D. Labeyrie, A. Juilletleclerc, and J. C. Duplessy (1988), A deep hydrological front between intermediate and deep-water masses in the glacial indian-ocean, *Nature*, *333*(6174), 651–655, doi:10.1038/333651a0.

Keeling, R. F., and B. B. Stephens (2001), Antarctic sea ice and the control of Pleistocene climate instability, *Paleoceanography*, *16*(1), 112–131, doi:10.1029/2000PA000529.

Keigwin, L. D. (2004), Radiocarbon and stable isotope constraints on Last Glacial Maximum and Younger Dryas ventilation in the western North Atlantic, *Paleoceanography*, *19*, PA4012, doi:10.1029/2004PA001029.

Kim, S.-T., and J. R. O'Neil (1997), Equilibrium and nonequilibrium oxygen isotope effects in synthetic carbonates, *Geochim. Cosmochim. Acta*, *61*(16), 3461–3475, doi:10.1016/S0016-7037(97)00169-5.

Knox, F., and M. B. McElroy (1984), Changes in atmospheric CO_2: Influence of the marine biota at high-latitude, *J. Geophys. Res.*, *89*(D3), 4629–4637, doi:10.1029/JD089iD03p04629.

Kunze, E., E. Firing, J. M. Hummon, T. K. Chereskin, and A. M. Thurnherr (2006), Global abyssal mixing inferred from lowered ADCP shear and CTD strain profiles, *J. Phys. Oceanogr.*, *36*(8), 1553–1576, doi:10.1175/JPO2926.1.

Large, W. G., and A. J. G. Nurser (2001), Ocean surface water mass transformation, in *Ocean Circulation and Climate: Observing and Modeling the Global Ocean*, *Int. Geophys. Ser.*, vol. 77, edited by G. Siedler, J. Church, and J. Gould, pp. 317–336, Academic, San Diego, Calif.

Ledwell, J. R., A. J. Watson, and C. S. Law (1998), Mixing of a tracer in the pycnocline, *J. Geophys. Res.*, *103*(C10), 21,499–21,529, doi:10.1029/98JC01738.

LeGrand, P., and C. Wunsch (1995), Constraints from paleotracer data on the North Atlantic circulation during the Last Glacial Maximum, *Paleoceanography*, *10*(6), 1011–1045, doi:10.1029/95PA01455.

LeGrande, A. N., and G. A. Schmidt (2006), Global gridded data set of the oxygen isotopic composition in seawater, *Geophys. Res. Lett.*, *33*, L12604, doi:10.1029/2006GL026011.

Lumpkin, R., and K. Speer (2007), Global ocean meridional overturning, *J. Phys. Oceanogr.*, *37*(10), 2550–2562, doi:10.1175/JPO3130.1.

Lynch-Stieglitz, J., W. B. Curry, and N. Slowey (1999), A geostrophic transport estimate for the Florida Current from the oxygen isotope composition of benthic foraminifera, *Paleoceanography*, *14*(3), 360–373, doi:10.1029/1999PA900001.

Marchal, O., and W. B. Curry (2008), On the abyssal circulation in the glacial Atlantic, *J. Phys. Oceanogr.*, *38*(9), 2014–2037, doi:10.1175/2008JPO3895.1.

Monnin, E., A. Indermuhle, A. Dallenbach, J. Fluckiger, B. Stauffer, T. F. Stocker, D. Raynaud, and J. M. Barnola (2001), Atmospheric CO_2 concentrations over the last glacial termination, *Science*, *291*(5501), 112–114, doi:10.1126/science.291.5501.112.

Morris, M. Y., M. M. Hall, L. C. St Laurent, and N. G. Hogg (2001), Abyssal mixing in the Brazil Basin, *J. Phys. Oceanogr.*, *31*(11), 3331–3348, doi:10.1175/1520-0485(2001)031<3331:AMITBB>2.0.CO;2.

Munk, W. (1966), Abyssal recipes, *Deep Sea Res.*, *13*, 707–730.

Neftel, A., H. Oeschger, J. Schwander, B. Stauffer, and R. Zumbrunn (1982), Ice core sample measurements give atmospheric CO_2 content during the past 40,000 yr, *Nature*, *295*(5846), 220–223, doi:10.1038/295220a0.

Ninnemann, U. S., and C. D. Charles (2002), Changes in the mode of Southern Ocean circulation over the last glacial cycle revealed by foraminiferal stable isotopic variability, *Earth*

Planet. Sci. Lett., *201*(2), 383–396, doi:10.1016/S0012-821X(02)00708-2.

Nurser, A. J. G., and M. M. Lee (2004), Isopycnal averaging at constant height. Part I: The formulation and a case study, *J. Phys. Oceanogr.*, *34*(12), 2721–2739, doi:10.1175/JPO2649.1.

Oppo, D. W., and S. J. Lehman (1993), Mid-depth circulation of the subpolar North Atlantic during the Last Glacial Maximum, *Science*, *259*(5098), 1148–1152, doi:10.1126/science.259.5098.1148.

Ostermann, D. R., and W. B. Curry (2000), Calibration of stable isotopic data: An enriched $\delta^{18}O$ standard used for source gas mixing detection and correction, *Paleoceanography*, *15*(3), 353–360, doi:10.1029/1999PA000411.

Plumb, R. A., and R. Ferrari (2005), Transformed Eulerian-mean theory. Part 1: Nonquasigeostrophic theory for eddies on a zonal-mean flow, *J. Phys. Oceanogr.*, *35*(2), 165–174, doi:10.1175/JPO-2669.1.

Polzin, K. L., J. M. Toole, J. R. Ledwell, and R. W. Schmitt (1997), Spatial variability of turbulent mixing in the abyssal ocean, *Science*, *276*(5309), 93–96, doi:10.1126/science.276.5309.93.

Robinson, L. F., J. F. Adkins, L. D. Keigwin, J. Southon, D. P. Fernandez, S. L. Wang, and D. S. Scheirer (2005), Radiocarbon variability in the western North Atlantic during the last deglaciation, *Science*, *310*(5753), 1469–1473, doi:10.1126/science.1114832.

Sarmiento, J. L., and J. R. Toggweiler (1984), A new model for the role of the oceans in determining atmospheric pCO_2, *Nature*, *308*(5960), 621–624, doi:10.1038/308621a0.

Schlosser, P., J. L. Bullister, and R. Bayer (1991), Studies of deep-water formation and circulation in the Weddell Sea using natural and anthropogenic tracers, *Mar. Chem.*, *35*(1–4), 97–122, doi:10.1016/S0304-4203(09)90011-1.

Siegenthaler, U., and T. Wenk (1984), Rapid atmospheric CO_2 variations and ocean circulation, *Nature*, *308*(5960), 624–626, doi:10.1038/308624a0.

Sigman, D. M., and E. A. Boyle (2000), Glacial/interglacial variations in atmospheric carbon dioxide, *Nature*, *407*(6806), 859–869, doi:10.1038/35038000.

Speer, K., and E. Tziperman (1992), Rates of water mass formation in the North Atlantic ocean, *J. Phys. Oceanogr.*, *22*(1), 93–104, doi:10.1175/1520-0485(1992)022<0093:ROWMFI>2.0.CO;2.

Speer, K. G., and W. Zenk (1993), The flow of antarctic bottom water into the Brazil basin, *J. Phys. Oceanogr.*, *23*(12), 2667–2682, doi:10.1175/1520-0485(1993)023<2667:TFOABW>2.0.CO;2.

Stammer, D. (1998), On eddy characteristics, eddy transports, and mean flow properties, *J. Phys. Oceanogr.*, *28*(4), 727–739, doi:10.1175/1520-0485(1998)028<0727:OECETA>2.0.CO;2.

Toggweiler, J. R. (1999), Variation of atmospheric CO_2 by ventilation of the ocean's deepest water, *Paleoceanography*, *14*(5), 571–588, doi:10.1029/1999PA900033.

Wunsch, C. (1996), *Ocean Inverse Problems*, Cambridge Univ. Press, Cambridge, U. K., doi:10.1017/CBO9780511629570.

Wunsch, C. (2003), Determining pale oceanographic circulations, with emphasis on the Last Glacial Maximum, *Quat. Sci. Rev.*, *22*(2–4), 371–385, doi:10.1016/S0277-3791(02)00177-4.

Zahn, R., and A. Mix (1991), Benthic foraminiferal $\delta^{18}O$ in the ocean's temperature-salinity-density field: Constraints on ice age thermohaline circulation, *Paleoceanography*, *6*(1), 1–20, doi:10.1029/90PA01882.

J. F. Adkins, Division of Geological and Planetary Sciences, California Institute of Technology, MC100-23, 1200 E. California Blvd., Pasadena, CA 91125, USA.

R. Ferrari, Department of Earth, Atmospheric, and Planetary Sciences, Massachusetts Institute of Technology, 77 Massachusetts Ave., Cambridge, MA 02139, USA.

D. C. Lund, Department of Geological Sciences, University of Michigan, 2534 CC Little Bldg., 1100 N. University Ave., Ann Arbor, MI 48109, USA. (dclund@umich.edu)